RESEARCH ARTICLE

Adaptive Voltage Control for Second-Order DC–DC Converters Supplying an Unknown Constant Power Load: A Generalized PBC Plus Damping Injection Design

WALTER GIL-GONZÁLEZ[1], (Senior Member, IEEE), **SEBASTIÁN RIFFO**[2],
OSCAR DANILO MONTOYA[3], (Senior Member, IEEE), **CARLOS RESTREPO**[2,4],
AND JESÚS C. HERNÁNDEZ[5], (Member, IEEE)

[1]Department of Electrical Engineering, Universidad Tecnológica de Pereira, Pereira 660003, Colombia
[2]Department of Electrical Engineering, Universidad de Talca, Curicó 3340000, Chile
[3]Facultad de Ingeniería, Universidad Distrital Francisco José de Caldas, Bogotá 110231, Colombia
[4]Principal Investigator Millennium Institute on Green Ammonia as Energy Vector (MIGA), Santiago 7820436, Chile
[5]Department of Electrical Engineering, University of Jaén, 23071 Jaén, Spain

Corresponding authors: Oscar Danilo Montoya (odmontoyag@udistrital.edu.co) and Jesús C. Hernández (jcasa@ujaen.es)

ABSTRACT This paper presents a generalized controller design to regulate the output voltage of second-order DC-DC converters feeding an unknown constant power load (CPL). Passivity-based control plus damping injection theory is employed to design a generalized action control to stabilize DC-DC converters. Furthermore, starting from the immersion and invariance (I&I) method, a generalized observer for second-order DC-DC converters is implemented to estimate the CPL value. By mixing the proposed controller with the I&I method, an adaptive generalized control approach is presented, which guarantees the locally asymptotic stability of the closed-loop for each converter. The main advantage of the nonlinear adaptive control design is its nonparametric dependence on the capacitance and inductance values, which makes it robust against parametric uncertainties. Phase portrait and sensitivity analyses are performed, and simulation and experimental results are examined to evaluate the performance of the proposed approach, which is also compared against feedback linearization and sliding mode control. Simulation and experimental results show the robustness and effectiveness of the adaptive proposed control approach.

INDEX TERMS Second-order DC–DC converters, constant power load, passivity-based control, damping injection design, adaptive generalized control, immersion and invariance.

NOMENCLATURE
Acronyms
AC	Alternating current.
CPL	Constant power load.
DC	Direct current.
FLC	Sliding mode control.
I&I	Immersion and invariance.
PBC	Passivity-based control.
pH	port-controlled Hamiltonian.
SMC	Feedback linearization control.

Parameters
$(\cdot)^\star$	Equilibrium point of the variables or control action.
γ_k	Coefficient for each converter configuration.

The associate editor coordinating the review of this manuscript and approving it for publication was Chi-Seng Lam.

λ	Positive gain of the I&I method.
C	Capacitance value.
K	Positive gain of the damping injection.
k_1, k_2, k_z	Control gains fo the FLC approach.
L	Inductance value.
P	Constant power load.
Q, λ, μ	Control gains fo the SMC approach.
R_1, R_2	Positive gains of the PBC.

Variables

$\hat{P}$	CPL estimated value.
ν	Damping injection action.
θ	Auxiliary variable of the I&I method.
$\tilde{P}$	CPL estimated error.
ξ	External vector.
E	Converter supply voltage.
H_d	Desired total stored energy.
i	Inductor current.
$J_d(x)$	Desired interconnection matrix.
$R_d(x)$	Desired dissipation matrix.
s	Switching surface of the SMC approach.
u	Control action.
v	Converter output voltage.
w	Auxiliary variable of the FLC approach.
x	State variable vector.
y_d	Desired passive output.
z	Auxiliary integral variable for the FLC or SMC approaches.

I. INTRODUCTION
A. GENERAL CONTEXT
In recent years, distribution systems have gone from passive electrical systems to active networks due to the advances made in renewable generation, energy storage systems, and controllable loads, all operated through efficient and intelligent management systems [1]. In addition, based on the advances in power electronic conversion technologies, distribution networks have also transformed into multiple microgrids interconnected with the main grid, which can operate with alternating current (AC) or direct current (DC) technologies [2], [3], [4]. Nowadays, DC systems have attracted the attention of researchers and industries due to their operational advantages in comparison with conventional AC technologies, namely their (i) minimal energy losses [5], (ii) excellent voltage profiles [6], and (iii) easy control design (no reactive power and frequency control requirements) [7]. The advantages of DC systems over their AC counterparts also pose significant challenges regarding operation and control, as power electronic converters for DC applications introduce nonlinearities in grid operation. Due to forced-commutated switches, these nonlinearities are added, along with the possible presence of multiple nonlinear loads connected into the DC microgrids [8], [9], [10].

Nonlinear loads in DC networks typically correspond to the constant power terminals, where the relation between voltages and powers takes a hyperbolic form [11], [12], [13], and

[14]. The main complication with hyperbolic terms for control applications in DC microgrids lies in the negative resistance effects that can cause instabilities during closed-loop operation [15]. Second-order DC-DC converters are typically used to integrate multiple constant power terminals into DC microgrids, namely buck, boost, buck-boost, and non-inverting buck-boost converters [16]. The main characteristic of these converter configurations is that they all produce two nonlinear differential equations with a stable equilibrium point [13], [16]. These operating points need to be stabilized using an effective nonlinear control design that guarantees stable closed-loop operation in the Lyapunov sense [13].

An additional challenge in designing controls for DC microgrid applications is that most control designs based on the system model require knowledge of the exact value of the constant power load. However, this is impractical in most cases since the load varies based on the user's consumption requirements [17]. Several tools have been developed to estimate online loads, which help to ensure asymptotic convergence. These estimators need to be integrated with nonlinear control designs to guarantee stable closed-loop operation of second-order DC-DC converters that interface with nonlinear constant power terminals [9].

B. MOTIVATION
The issue of control for second-order DC-DC converters that interface with constant power terminals is a common research topic in specialized literature. Most control designs focus solely on a specific control application, which can make it challenging to apply them to all classical second-order DC-DC topologies [16]. In addition, the presence of nonlinear loads complicates the design of controllers due to stability requirements in closed-loop operation. As a result, some authors avoid in-depth analyses of this topic and instead focus on typical linearization designs based on Laplace implementations [18]. These designs can function effectively in a variety of operating scenarios. However, these methods cannot guarantee global stability properties and should only be used in local designs where the constant power load experiences minimal variations. Other authors have implemented control using nonlinear methods such as passivity-based control, exact feedback control, and sliding mode control. These methods ensure stability properties in the sense of Lyapunov during closed-loop operation [8], [9], [19]. Even though these controllers are efficient, they rely heavily on the parameters of second-order DC-DC converters, *i.e.*, inductors and capacitors. This dependence on accurate estimation can lead to unexpected oscillations around the operation point, making these controllers less reliable. This occurs when capacitors and inductors experience significant deviations from their nominal values [20].

Motivated by the significant challenges posed by designing controllers for DC-DC converters that integrate constant power terminals with unknown values, this research proposes an efficient control methodology. The proposed methodology

ensures stability properties in the sense of Lyapunov, regardless of the converter parameters. It allows for online load estimation without affecting stability.

C. STATE OF THE ART REVIEW

Several approaches have been proposed for controlling second-order DC-DC converters that supply a constant power load (CPL). Multiple control methods have been studied for DC-DC buck converters. In [21], a sliding mode control (SMC) was presented to stabilize and regulate the output voltage in a buck converter. In [22], a fuzzy logic method was proposed in order to ensure the stabilization of the buck converter with changes in CPL. [23] presented a composite model predictive control (MPC) approach to regulate the output voltage in buck converters that supply a CPL. The study by [24] proposed a H_∞-based control approach to ensure the proper operation of a buck converter. The H_∞-based control utilizes the Glover-Doyle optimization algorithm in order to determine the optimal control law. In [8], a passivity-based control (PBC) with proportional-integral (PI) action was proposed to ensure stable operation of DC-DC buck converters. The authors of [25] conducted a study on an adaptive energy shaping method applied to a buck converter in a DC microgrid. In [26], an adaptive power shaping control was described for regulating the voltage of buck converters. This control did not utilize the measurement of the CPL, which was estimated using the immersion and invariance (I&I) method. However, the control law depends on the parameters of the converter. The authors of [27] utilized the Kharitonov theorem to develop a robust proportional-integral-derivative (PID) controller for a buck converter. In [28], a hybrid approach that combines the Markov decision process and deep Q-network algorithms was employed to regulate buck converters using deep reinforcement learning. In [29], a second-order SMC approach was used to regulate the output voltage of a buck converter while supplying power to a CPL. This approach requires measuring the CPL and having knowledge of the parameters of the converter. The study by [30] implemented a robust approach based on RST digital feedback to regulate the output voltage of a buck converter that supplies a CPL. Finally, the authors of [31] proposed an adaptive multiagent-based control strategy to manage the flexible voltage regulation in a DC microgrid. This control was applied to the DC-DC buck converter for the photovoltaic system and the bidirectional DC-DC buck converter for the battery energy storage system. Some parts of the DC microgrid were considered CPL, and others were a constant power source representing renewable energy systems. However, the classical PI controls were used to regulate the voltage and current in the converters, which is not possible to guarantee the system's stability.

In the case of DC-DC boost converters, several control methods have also been utilized. In [19], a robust SMC-based pulse-width modulation (PWM) method was proposed to mitigate the instabilities caused by the CPL in DC microgrids.

In [32], a stability analysis was conducted on a boost converter that was connected to a battery energy storage system and fed a CPL. [33] proposed an adaptive backstepping SMC approach to regulate the output voltage of a boost converter connected to a CPL. In [34] and [35], an incremental PBC was presented to control a DC-DC converter in the presence of time-varying disturbances. These disturbances were effectively rejected using a PI observer. In [36], an SMC approach was presented for regulating a boost converter that supplies power to a CPL. The authors employed a linear switching surface to reduce the inrush current in the boost converter and maintain its output voltage at the desired level, even in the presence of external disturbances. In [37], a robust type-II fuzzy method based on PWM was proposed for a DC-DC boost converter supplying a CPL. [38] presented a finite-time parameter observer-based SMC method to manage the output voltage of a DC-DC boost converter with a CPL. The authors of [39] described an adaptive output feedback approach for controlling a DC-DC boost converter. This approach involves using a reduced-order state observer to estimate the inductor current and load conductance of the converter. In [40], a PI-PBC approach was proposed to stabilize the output voltage of a DC-DC converter. This approach was combined with a parameter estimation-based observer to estimate the current flowing through the converter inductor. The study by [41] described a global tracking, sensorless PI-PBC approach to regulate the output voltage of a DC-DC boost converter connected to a DC microgrid. The authors of [42] proposed a sensorless PI+PBC approach in a DC-DC converter in order to control its output voltage while it feeds a CPL.

Multiple controllers have been proposed for DC-DC buck-boost converters. In [43], an adaptive energy shaping control for output voltage regulation of DC-DC buck-boost converters feeding unknown CPLs was presented. In [44], an interconnection and damping assignment (IDA) control based on PBC theory was introduced in order to regulate the output voltage of DC-DC buck-boost converters with a CPL of unknown power. This controller used the I&I method and was transformed into an adaptive approach. The work by [45] used a deep machine-learning technique to control DC-DC buck-boost converters with a CPL. This technique employed the Actor-Critic architecture and incorporated ultra-local model control to tackle the instability effect caused by CPLs under reference voltage changes. In [46], an intelligent feedback controller based on a deep deterministic policy gradient was presented to regulate the output voltage of a buck-boost converter feeding CPLs via wireless power transfer applications. The intelligent feedback controller was combined with a sliding mode observer to alleviate the unknown dynamics of the converter. The study by [47] introduced an interconnection and damping assignment control based on passivity theory to manage the output voltage in DC-DC buck-boost converters supplying an unknown CPL. In [48], an MPC approach was performed for stabilizing DC-DC buck-boost converters feeding a CPL. The research by [49] proposed a robust nonlinear

controller for stabilizing the output voltage in DC-DC buck-boost converters. Said control was based on PI actions, and its stability was ensured using a Lyapunov function. Furthermore, controllers such as feeding-back control [50], the SMC approach [51], the robust SMC approach [52], digital schemes [53], and optimal design [54] have been described. For DC-DC non-inverting buck-boost converters, the authors of [55] described a nonlinear backstepping controller to extract maximum power from photovoltaic systems. Finally, in [56], a fuzzy logic controller for DC-DC non-inverting buck-boost converters was presented.

All controllers mentioned above have exhibited good performance, some of which can be regarded as robust. However, some of them can be difficult to implement and require knowledge of all converter states, load conditions, and system parameters. There are many parameters to be tuned, and an online optimization process must be performed. These controllers are designed and applied to a specific converter, which does not allow the action control to be easily changed to another type of second-order DC-DC converter. Even so, it is essential to mention that, in the studies by [16] and [57] the proposed controls for all second-order DC-DC converters only considered resistive loads, which is an easy problem to solve. Unlike these previous works, this paper proposes a generalized adaptive voltage control for DC-DC converters supplying an unknown CPL. Said control is based on the PBC approach, which can ensure local stability in a closed loop. Furthermore, it adds a damping injection design to impose the desired damping in order to achieve the desired controlled dynamics. Additionally, the proposed controller does not depend on the converter parameters and does not require measuring the estimated CPL.

D. CONTRIBUTIONS AND SCOPE

Based on the comprehensive review of state of the art regarding control design for second-order DC-DC converter applications, this research makes the following contributions:

i. The design of a general nonlinear controller based on PBC plus damping action, which works in each of the four classical DC-DC converter topologies. It is only necessary to change some coefficients from 0 to 1 or *vice versa* in order to apply the proposed control law to any converter considered in this study. Furthermore, the proposed controller works with an online load estimator in order to make it adaptive, and it does not require measurement. The main advantage of the proposed general controller is that it is completely independent of the converter parameters; it is robust against parametric uncertainties.

ii. A generalized power constant load estimator based on the I&I method. This estimator can reach the CPL value for any converter used in this paper.

iii. A comparison between the proposed controller design against efficient nonlinear controllers based on the SMC and feedback linearization control (FLC) approaches. These have been designed for all of the second-order

DC-DC converter topologies under study, as well as to ensure stable properties in the sense of Lyapunov for closed-loop operation. These controllers are also operated simultaneously with the online load estimator. Phase portraits, simulations, and experiment results confirm the proposed general controller's effectiveness when compared to the SMC and FLC designs.

It is imperative to mention that, in the context of this study, the models of the four DC-DC converters have been derived in the continuous domain, *i.e.*, using the average modeling theory. Furthermore, the resistive effects of inductors, capacitors, and switches are disregarded in the analysis. This is because the absence of said effects represents the most unfavorable operating conditions for stability in a closed loop, as they introduce damping and generate energy dissipation, improving the dynamic responses of the converters.

E. DOCUMENT STRUCTURE

The remainder of this paper is structured as follows. Section II describes the design of the general passivity-based controller, including damping injection. Section III describes the general modeling for the four DC-DC converters studied using the averaging modeling theory. Then, Section IV shows the adaptive PBC design with including the damping injection. This design shows the independence of the proposed controller regarding the converter parameters. Section V presents all computational analyses, simulations, and experimental implementations carried out in this study, as well as a complete comparison with the FLC and SMC approaches. Finally, Section VI lists the main conclusions derived from this research and some possible future research developments.

II. PASSIVITY-BASED CONTROL METHOD

Passivity-based control (PBC) theory is a field of nonlinear control theory that focuses on a particular class of dynamical systems with port-Hamiltonian modeling [61], with the main advantage that stability, even local or global, can be ensured by preserving the pH properties of the system during closed-loop operation [62]. An additional advantage of PBC theory is that control actions have a physical meaning, which corresponds to the dynamical system's energy flow redistribution by modifying the interconnection between state variables and adding the desired energy dissipation/damping [61]. PBC theory has multiple variants regarding control design. Come of them are interconnection and damping (IDA-PBC) [63], energy shaping PBC [64], standard PBC [62], and proportional-integral PBC (PI-PBC) [65], among others. The selection of each PBC variant depends on the control requirements and the specific structure of the dynamical system under analysis. In the case of power electronic converters and their applications, the most conventional PBC designs are IDA-PBC and PI-PBC [3], [63]. However, selecting each of these methods for power electronic converters strictly depends on the load connection, given that PI-PBC design is only suitable for purely bilinear systems with linear loads, *i.e.*, the only permitted nonlinearities are the

TABLE 1. Summary of the controllers applied of the second-order DC-DC converters.

Control method	Type of converter	Type of load	Load est.	Year	Ref.
Sliding mode control	Buck	CPL load	✗	2014	[21]
Fuzzy logic control	Buck	CPL load	✗	2017	[22]
Model predictive control	Buck	CPL load	✓	2019	[23]
H_∞-based control	Buck	CPL load	✓	2020	[24]
Adaptive power shaping control	Buck	CPL load	✓	2021	[26]
Passivity-based control	All	Linear load	✓	2021	[16]
Robust PID controller	Buck	CPL load	✗	2021	[27]
Second-order SMC approach	Buck	CPL load	✓	2022	[29]
Inverse optimal control	All	Linear load	✗	2022	[57]
Robust sliding mode control	Boost	CPL load	✗	2015	[19]
Dual PI controller	Boost	CPL and linear load	✗	2015	[32]
Incremental passivity-based controller	Boost	Linear load	✗	2016, 2018	[34], [35]
Sliding predictive control	Boost	Linear load	✓	2018	[58]
Adaptive backstepping SMC	Boost	CPL	✗	2019	[33]
Sliding mode control	Boost	CPL	✗	2019	[36]
PI passivity-based control	Boost	CPL	✓	2021	[40]
Robust Inverse Optimal Control	Boost	Linear load	✗	2021	[59]
Backstepping control	Boost	CPL and linear load	✗	2022	[60]
Sensroless PI-PBC	Boost	CPL and linear load, CPL	✓	2022	[41], [42]
Robust SMC approach	Buck-boost	Linear load	✗	2016, 2017	[51], [52]
Adaptive energy shaping control	Buck-boost	CPL	✓	2018	[43]
Adaptive IDA-PBC	Buck-boost	CPL	✓	2019, 2020	[44], [47]
Model predictive control	Buck-boost	CPL	✗	2021	[48]
Robust nonlinear PI-type controller	Buck-boost	Linear load	✗	2022	[49]
Backstepping controller	Non-inverting Buck-boost	Linear load	✗	2020	[55]
Fuzzy logic controller	Non-inverting Buck-boost	Linear load	✗	2020	[56]
This paper	**All**	**CPL load**	✓	2023	—

bilinear ones. In contrast, IDA-PBC design is more general and allows working with nonlinear loads modeled as constant power terminals, as is the case of this research. Note that, in this research, IDA-PBC and pure PBC are used indistinctly for the sake of simplicity.

The general design of a controller using the PBC approach is described below for a general nonlinear dynamical system.

$$\dot{x} = f(x) + g(x)u. \tag{1}$$

Considering that PBC theory is specially designed for nonlinear dynamical systems with pH structure, the general nonlinear system (1) is presented as a pH system in (2).

$$\dot{x} = [J(x) - R(x)] \nabla H + g(x)u + \xi,$$
$$y = g(x)^\top \nabla H, \tag{2}$$

where $x\, \xi \in R^n$ are the state variables and the external vector, respectively; $H : R^n \longrightarrow R$ represents the system's total stored energy; $u \in R^m$ is the control action with $m < n$; $J(x) = -J(x)^\top \in R^{n \times n}$ is the internal interconnection matrix; $R(x) = R(x)^\top \geq 0 \in R^{n \times n}$ is the internal dissipation matrix; and $g(x)$ is the input matrix.

The PBC method proposes a control action via a feedback loop (*i.e.*, by adding interconnection and damping) which leads to the closed-loop system taking a pH structure [61]:

$$\dot{x} = [J_d(x) - R_d(x)] \nabla H_d, \tag{3}$$

where $J_d(x) = -J_d(x)^\top$ and $R_d(x) = R_d(x)^\top \geq 0$ are the desired internal interconnection and dissipation matrices

in a closed loop, and H_d represents the desired total energy stored [61], [62], such as

$$x^\star = \arg \min H_d(x) \tag{4}$$

with $x^\star \in R^n$ being the desired equilibrium point. Then, the closed-loop system in (3) is reached with the control action $u = \beta(x)$, where

$$\beta(x) = \mathcal{G} \begin{bmatrix} [J_d(x) - R_d(x)] \nabla H_d \\ -[J(x) - R(x)] \nabla H - \xi \end{bmatrix}, \tag{5}$$

with $\mathcal{G} = [g(x)^\top g(x)]^{-1} g(x)^\top$.

The equilibrium point $x^\star$ for non-controlled state variables is determined after supposing a function H_d and fixing the matrices $g(x)^\perp$, $J_d(x)$, and $R_d(x)$, which validates [61], [62]:

$$g(x)^\perp \begin{pmatrix} [J_d(x) - R_d(x)] \nabla H_d - \\ [J(x) - R(x)] \nabla H - \xi \end{pmatrix} = 0, \tag{6}$$

where $g(x)^\perp$ is a full-rank left annihilator of $g(x)$ that meets $g(x)^\perp g(x) = 0$ and (4).

Remark 1: It is important to mention that the full-rank left annihilator $g(x)^\perp$ eliminates the control input u and computes the non-controlled variables of the system in closed-loop operation [62].

A. DAMPING INJECTION
Over the action control, it is possible to add damping injection, which allows imposing a desired damping, thus improving the convergence of specific variables. To this effect, the

control action (5) with damping injection (v) is defined as $u = \beta(x) + v$, where

$$v = -Ky_d = -Kg(x)^\top \nabla H_d, \qquad (7)$$

with $K = K^\top > 0$ when

$$\lim_{t \to \infty} y_d(t) = 0 \Rightarrow g(x(t))^\top \nabla H_d(x(t)) = 0. \qquad (8)$$

The control action $u = \beta(x) + v$ causes the system (2) to take the following pH structure in a closed loop:

$$\dot{x} = [J_d(x) - R_d(x)] \nabla H_d - g(x)Kg(x)^\top \nabla H_d. \qquad (9)$$

B. STABILITY ANALYSIS

The desired total stored energy H_d qualifies as a Lyapunov function, which is defined as

$$W(x - x^\star) = H_d. \qquad (10)$$

This complies with $W(x - x^\star) > 0 \; \forall \; x \neq x^\star$ and $W(x = x^\star) = 0$. Furthermore, the temporal derivative of the Lyapunov function is

$$
\begin{aligned}
\dot{W}(x - x^\star) &= \nabla H_d^\top \dot{x} \\
&= \nabla H_d^\top \left[J_d(x) - R_d(x) - g(x)Kg(x)^\top \right] \nabla H_d \\
&= -\nabla H_d^\top R_d(x)\nabla H_d - y_d^\top K y_d \\
&= -\nabla H_d^\top R_d(x)\nabla H_d.
\end{aligned} \qquad (11)
$$

The pH dynamical system (2) is locally stable at the equilibrium point with control action $u = \beta(x) + v$ if $R_d(x) \geq 0$ ($\dot{W} \leq 0$) (see [66] for more details on Lyapunov's theorem).

III. DYNAMIC MODELING FOR SECOND-ORDER DC-DC CONVERTERS

This section describes a general dynamic model for all classic second-order DC-DC converters considered in the paper, *i.e.*, buck, boost, buck-boost, and non-inverting buck-boost converters. This group of converters is illustrated in Fig. 1 while feeding a CPL. They have two dynamics related to their inductor and capacitor, which is why they are classified as second-order converters [16]. The following practical assumptions are made for this group of converters:

Assumption 1: The supply voltage $E \in R_{>0}$, the inductor current $i \in R_{>0}$, and the output voltage $v \in R_{>0}$ are measurable ($-v > 0$ for buck-boost converter). For the sake of simplicity, the current and voltage in the converters are denoted as $x_1 := Li$ and $x_2 := Cv$, respectively.

Assumption 2: The parameters of the DC-DC converter are positive ($L > 0$ and $C > 0$).

Assumption 3: The CPL P is bounded and positive ($0 < P \leq P^{\max}$).

Assumption 4: The switching frequency is high enough to assume the average model for DC-DC converters. Hence, the control action u is defined as $u \in [0, 1]$.
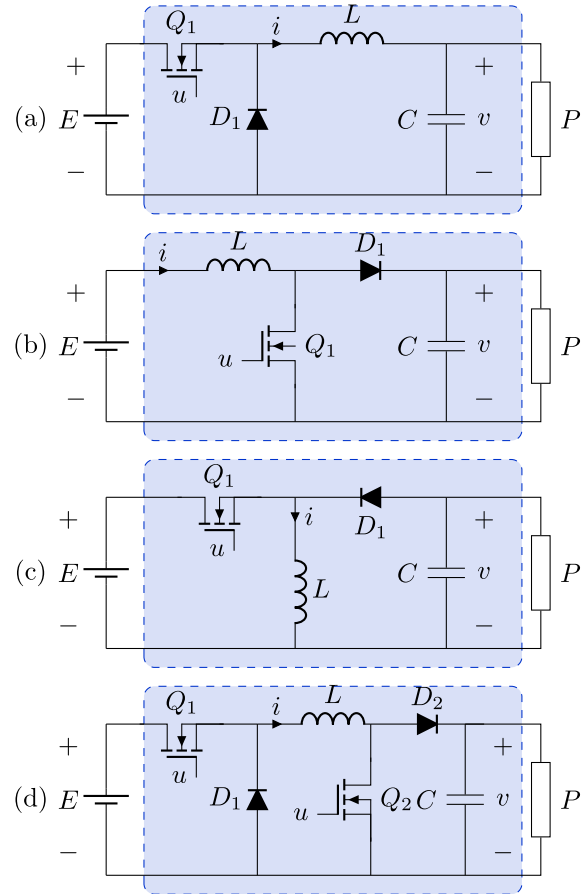

FIGURE 1. Topologies of second-order DC-DC converters feeding a CPL: (a) buck, (b) boost, (c) buck-boost, and (d) on-inverting buck-boost

A. BUCK CONVERTER DYNAMIC MODELING

Fig. 1a presents a buck converter, also known as a *step-down converter*. This is because its output voltage is lower than its supply voltage, which means that its output current is higher than its input current. Buck converters are generally implemented in applications that regulate the output voltage under load variations [8].

The buck converter's dynamical system is obtained by applying Kirchhoff's first law to the mesh that is formed with the inductor and Kirchhoff's second law to the node that connects with the capacitor as shown in Fig. 1a, thus reaching the following dynamical model

$$
\begin{aligned}
L\dot{i} &= -v + uE, \\
C\dot{v} &= i - \frac{P}{v}.
\end{aligned} \qquad (12)
$$

The equilibrium set of the dynamical system (12) is straightforwardly defined as

$$\varepsilon := \left\{ (i, v) \in R_{>0}^2 \mid i - \frac{P}{v} = 0 \right\}. \qquad (13)$$

Hence, the desired equilibrium point for $i^\star$ with a given $v^\star$ is

$$i^\star = \frac{P}{v^\star}. \tag{14}$$

B. BOOST CONVERTER DYNAMIC MODELING

Fig. 1b depicts a boost converter, also called a *step-up converter*, as it can an output voltage higher than its supply voltage. This causes the output current to be less than the input current. This type of converter is usually employed to regulate the output voltage under load variations [36].

Similar to the buck converter, the boost converter's dynamical system (see Fig. 1b) is obtained by applying Kirchhoff's laws:

$$L\dot{i} = -(1-u)\,v + E,$$
$$C\dot{v} = (1-u)\,i - \frac{P}{v}. \tag{15}$$

The equilibrium set for the boost converter (15) is easily determined as

$$\varepsilon := \left\{(i,\ v) \in R_{>0}^2 \mid iE - P = 0\right\}. \tag{16}$$

Hence, the desired equilibrium point is

$$i^\star = \frac{P}{E}. \tag{17}$$

C. BUCK-BOOST CONVERTER DYNAMIC MODELING

Fig. 1c illustrates a buck-boost converter, which can regulate its output voltage at levels lower or higher than its supply voltage. The main feature of this type of converter is that its output voltage has an opposite polarity with respect to its supply voltage [46]. A buck-boost converter's dynamical system (see Fig. 1c) is also obtained via Kirchhoff's laws:

$$L\dot{i} = (1-u)\,v + uE,$$
$$C\dot{v} = -(1-u)\,i - \frac{P}{v}. \tag{18}$$

The equilibrium set for the dynamic system (18) is straightforwardly determined as

$$\varepsilon := \left\{(i,\ -v) \in R_{>0}^2 \mid i - P\left(\frac{1}{E} - \frac{1}{v}\right) = 0\right\}. \tag{19}$$

Thus, the desired equilibrium point for $i^\star$ with fixed $v^\star$ is

$$i^\star = P\left(\frac{1}{E} - \frac{1}{v^\star}\right). \tag{20}$$

D. NON-INVERTING BUCK-BOOST CONVERTER DYNAMIC MODELING

Fig. 1d shows a non-inverting buck-boost converter, which just as the buck-boost one, can manage its output voltage at levels lower or higher than its supply voltage. However, in this case, the output voltage maintains the same polarity as the supply voltage [16]. The non-inverting buck-boost

TABLE 2. γ-coefficient for each converter configuration.

Converter	γ_1	γ_2	γ_3	γ_4
Buck	1	0	1	0
Boost	1	1	0	1
Buck-boost	-1	-1	1	0
Non-inverting buck-boost	1	1	1	0

converter's dynamical system (see Fig. 1d) is reached by applying Kirchhoff's laws, as follows:

$$L\dot{i} = -(1-u)\,v + uE,$$
$$C\dot{v} = (1-u)\,i - \frac{P}{v}. \tag{21}$$

The equilibrium set for the non-inverting buck-boost converter (21) is easily defined as

$$\varepsilon := \left\{(i,\ v) \in R_{>0}^2 \mid i - P\left(\frac{1}{E} + \frac{1}{v}\right) = 0\right\}. \tag{22}$$

Thus, the desired equilibrium point for $i^\star$ with a fixed $v^\star$ is

$$i^\star = P\left(\frac{1}{E} + \frac{1}{v^\star}\right). \tag{23}$$

E. GENERAL DYNAMIC MODELING FOR SECOND-ORDER DC-DC CONVERTERS

The four second-order DC-DC converters presented above can be represented in a unique pH structure by employing a γ-coefficient that allows switching in each one of the configurations, as presented in Fig. 1. The general pH structure for second-order DC-DC converters can be defined as

$$\dot{x} = (\gamma_1 J - R)\nabla H + g(x)u + \gamma_4 \xi, \tag{24}$$

with $x = [x_1,\ x_2]^\top, \xi = [E,\ 0]^\top$ and

$$J = \begin{bmatrix} 0 & -1 \\ 1 & 0 \end{bmatrix},\ R = \begin{bmatrix} 0 & 0 \\ 0 & \frac{C^2 P}{x_2^2} \end{bmatrix},\ g(x) = \begin{bmatrix} \gamma_2 \frac{x_2}{C} + \gamma_3 E \\ -\gamma_2 \frac{x_1}{L} \end{bmatrix}.$$

The γ-coefficient for each converter configuration is listed in Table 2. Note that the total energy stored for the dynamical system (24) can be defined as

$$H = x^\top M x, \tag{25}$$

where

$$M = \begin{bmatrix} L & 0 \\ 0 & C \end{bmatrix}^{-1}.$$

IV. ADAPTIVE PBC PLUS DAMPING INJECTION DESIGN

This section presents the design of the adaptive PBC plus damping injection technique applied to the general dynamic modeling of the second-order DC-DC converters shown in (24). The control objective is to regulate the converters' output voltage, considering that they feed constant power terminals. Initially, it is assumed that the value of the CPL

(*i.e.*, P) is known and that the desired equilibrium point is assignable - in other words, that it exists.

In order to implement the PBC plus damping injection method described in Section II, it is required to fix the desired total energy stored (H_d) and the desired internal interconnection (J_d) dissipation (R_d) matrices.

Initially, H_d is defined as the quadratic function containing the parameters of the components that store energy in the converters:

$$H_d = (x - x^\star)^\top M(x - x^\star). \tag{26}$$

Its derivative with respect to time is

$$\dot{H}_d = \nabla H_d^{\top} \dot{x}. \tag{27}$$

Now, the desired J_d and R_d matrices are fixed as follows:

$$J = \begin{bmatrix} 0 & -1 \\ 1 & 0 \end{bmatrix}, \quad R = \begin{bmatrix} R_1 & 0 \\ 0 & R_2 \frac{C^2 P}{x_2^2} \end{bmatrix},$$

where $R_1 > 0$ and $R_2 > 0$.

Via (5) and (7), it is possible to calculate $\beta(x)$ and ν for the general control action $u = \beta(x) + \nu$:

$$\beta(x) =$$
$$- \frac{\left(\gamma_3 E + \gamma_2 \frac{x_2}{C}\right)\left(\frac{x_2 - x_2^\star}{C} + \gamma_4 E + \frac{R_1(x_1 - x_1^\star)}{L} - \gamma_1 \frac{x_2}{C}\right)}{\left(\gamma_3 E + \gamma_2 \frac{x_2}{C}\right)^2 + \left(\gamma_2 \frac{x_1}{L}\right)^2}$$
$$- \frac{\gamma_2 \frac{x_1}{L}\left(\frac{(x_1 - x_1^\star)}{L} + \frac{CP}{x_2} - \gamma_1 \frac{x_1}{L} - \frac{CPR_2(x_2 - x_2^\star)}{x_2^2}\right)}{\left(\gamma_3 E + \gamma_2 \frac{x_2}{C}\right)^2 + \left(\gamma_2 \frac{x_1}{L}\right)^2}, \tag{28}$$

$$\nu = -K \frac{\left(\gamma_3 E + \gamma_2 \frac{x_2}{C}\right)(x_1 - x_1^\star)}{L}$$
$$- K \frac{\gamma_2 x_1 (x_2 - x_2^\star)}{LC}. \tag{29}$$

Now, it is necessary to compute the non-controlled variable $x_1^\star$ in order to implement the general control action. Defining the left annihilator $g(x)^\perp$ as

$$g(x)^\perp = \left[\gamma_2 \frac{x_1}{L}, \ \gamma_2 \frac{x_2}{C} + \gamma_3 E\right], \tag{30}$$

and using (6), the non-controlled variable is

$$x_1^\star = -\frac{L^2 \sigma_4 \left(\gamma_1 \frac{x_1}{L} - \frac{CP}{x_2} + \gamma_2 \sigma_1 \frac{x_1}{L} + \sigma_3 - \frac{x_1}{L}\right)}{L\sigma_4 - \gamma_2 R_1 x_1}$$
$$+ \frac{\gamma_1 L x_1 \left(R_1 \frac{x_1}{L} + \gamma_4 E + \frac{x_2 - x_2^\star}{C} - \gamma_1 \frac{x_2}{C} - \sigma_1 \sigma_4\right)}{L\sigma_4 - \gamma_2 R_1 x_1}, \tag{31}$$

with

$$\sigma_1 = \frac{\sigma_4 \left(\frac{x_2 - x_2^\star}{C} + \alpha_4 E + R_1 \frac{x_1}{L} - \gamma_1 \frac{x_2}{C}\right)}{\sigma_2}$$
$$+ \frac{\gamma_2 \frac{x_1}{L}\left(\frac{x_1}{L} + \frac{CP}{x_2} - \gamma_1 \frac{x_1}{L} - \sigma_3\right)}{\sigma_2},$$
$$\sigma_2 = \sigma_4^2 + \left(\gamma_2 \frac{x_1}{L}\right)^2, \quad \sigma_3 = CPR_2 \frac{x_2 - x_2^\star}{C},$$
$$\sigma_4 = \alpha_3 E + \alpha_2 \frac{x_2}{C}.$$

A. POWER CONSTANT LOAD ESTIMATOR

The main difficulty in implementing the general control action for the proposed PBC plus damping injection controller is its dependence on knowing the CPL value, which may not be practical in real applications [9]. This is because the CPL value varies as a function of the load requirements. Therefore, it is necessary to apply a method that allows observing the load value at any time - also called an *estimator*.

Now, the general CPL estimator based on the I&I method is described [67]. Thus, it is assumed that the CPL value is unknown. The I&I method is an observer that estimates the CPL value while ensuring exponential convergence. The estimate error for CPL is defined as

$$\tilde{P} = \hat{P} - P, \tag{32}$$

where $\hat{P}$ is the estimated CPL value and is assumed as

$$\hat{P} = \theta - \frac{1}{2C}\lambda x_2^2, \tag{33}$$

with

$$\dot{\theta} = \lambda \frac{x_1 x_2}{LC}(\gamma_1 - \gamma_2 u) + \lambda \hat{P}, \tag{34}$$

where $\lambda > 0$ is the observer gain.

Now, taking the derivative with respect to the time of the estimated error $\tilde{P}$ yields

$$\dot{\tilde{P}} = \dot{\hat{P}} = \dot{\theta} - \frac{1}{C}\lambda x_2 \dot{x}_2 \dot{\tilde{P}} = \lambda \frac{x_1 x_2}{LC}(\gamma_1 - \gamma_2 u) - \lambda \hat{P}$$
$$\quad - \frac{1}{C}\lambda x_2 \left((\gamma_1 - \gamma_2 u)\frac{x_1}{L} - \frac{CP}{x_2}\right)$$
$$\dot{\tilde{P}} = \lambda \frac{x_1 x_2}{LC}(\gamma_1 - \gamma_2 u) - \lambda \hat{P}$$
$$\quad - \lambda \frac{x_1 x_2}{LC}(\gamma_1 - \gamma_2 u) + \lambda\left(\hat{P} - \tilde{P}\right)$$
$$\dot{\tilde{P}} = -\lambda \tilde{P} \tag{35}$$

By solving (35), the following is obtained:

$$\tilde{P}(t) = \tilde{P}(0)\exp^{(-\lambda t)}. \tag{36}$$

This indicates that

$$\lim_{t \to \infty} \tilde{P}(t) = 0 \Rightarrow \hat{P} = P, \tag{37}$$

which demonstrates that $\tilde{P}(t)$ goes to zero for any initial condition $\tilde{P}(0)$ and that its convergence is exponential.

B. ADAPTIVE CONTROL DESIGN

The general control action, considering the estimate $\hat{P}$ and recovering the original variables, takes the following form:

$$
\begin{cases}
u &= \beta(x) + v, \\
\beta(x) &= -\dfrac{\sigma_1 \left(v - v^\star + \gamma_4 E + R_1(i - i^\star) - \gamma_1 v \right)}{\sigma_2} \\
&\quad - \dfrac{\gamma_2 i \left((i - i^\star) + \frac{\hat{P}}{v} - \gamma_1 i - \frac{\hat{P} R_2 (v - v^\star)}{v^2} \right)}{\sigma_2}, \\
v &= -K \left(\sigma_1 \left(i - i^\star \right) - \gamma_2 i \left(v - v^\star \right) \right), \\
i^\star &= \dfrac{\gamma_2 i \left(\sigma_1 \sigma_4 + v^\star - (\gamma_1 - 1) v - R_1 i - \gamma_4 E \right)}{\sigma_1 - \gamma_2 R_1 i} \\
&\quad + \dfrac{\sigma_1 \left((1 - \gamma_1 - \gamma_2 \sigma_4) i - \sigma_3 \right)}{\sigma_1 - \gamma_2 R_1 i}, \\
\sigma_1 &= \gamma_3 E + \gamma_1 v, \\
\sigma_2 &= \sigma_1^2 + (\gamma_2 i)^2, \\
\sigma_3 &= \hat{P} R_2 \dfrac{v - v^\star}{v^2}, \\
\sigma_4 &= \dfrac{\gamma_1 \left(v - v^\star + R_1 i - \gamma_1 v + \gamma_4 E \right)}{\sigma_2} + \\
&\quad \dfrac{\gamma_2 i \left((1 - \gamma_1) i + \frac{\hat{P}}{v} - \sigma_3 \right)}{\sigma_2}, \\
\hat{P} &= \theta - \dfrac{1}{2} \lambda C v^2, \\
\dot{\theta} &= \lambda i v \left(\gamma_1 - \gamma_2 u \right) - \lambda \hat{P}.
\end{cases}
\tag{38}
$$

Fig. 2 illustrates the scheme of the adaptive generalized PBC plus damping injection design. Note that the only place where the converter parameters (capacitance) appear is the constant power load estimator. However, knowing the exact value of the capacitance is unnecessary, since the gain of the λ estimator can compensate for this.

The proposed control design has the following advantages: (i) the PBC theory finds a locally stable feedback control law that preserves the pH structure of the converters in an open-loop operation scenario by strengthening their interconnection structure and adding enough damping to allow reaching the desired closed-loop behavior; (ii) the controller design does not depend on the converter parameters, since, when the original variables are recovered, *i.e.*, $i = \frac{x_1}{L}$ and $\frac{x_2}{C}$, the inductance and capacitance values vanish, as shown in (38) (this is one of the most important advantages of the controller design because it makes it robust against parametric uncertainties); and (iii), even though the I&I load estimator is well-known for DC-DC converter applications, combining it with the proposed PBC controller results in a nonlinear adaptive controller that is general for the four analyzed DC-DC converter topologies (this has not yet been presented in the current literature and constitutes the main contribution of this research).

V. SIMULATIONS AND EXPERIMENTAL RESULTS

This section presents the performance analysis of the adaptive PBC plus damping injection approach, as shown in Section IV. From this point forward, this approach is referred
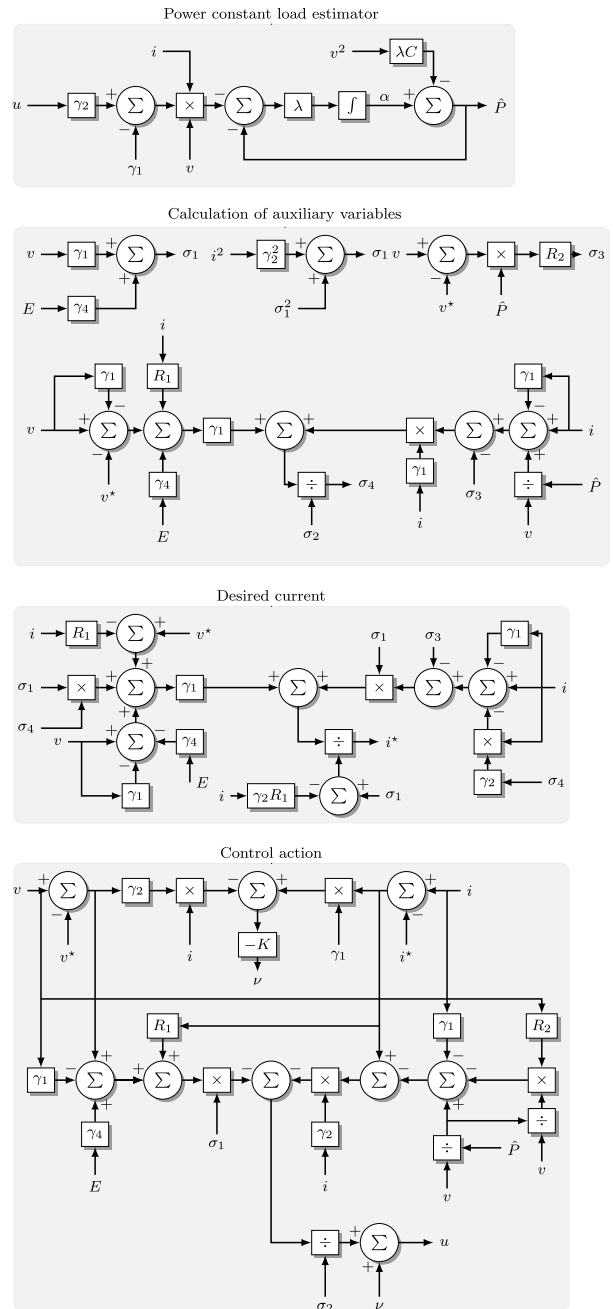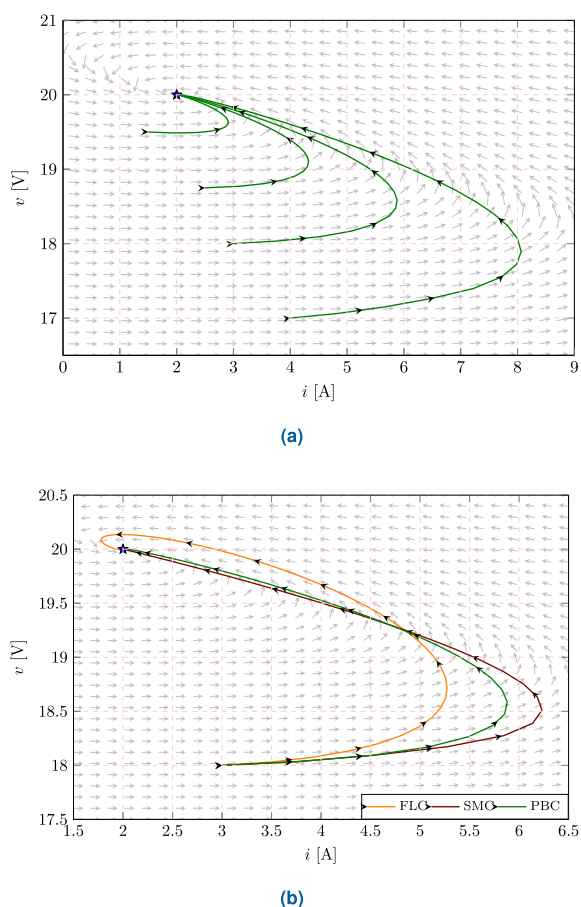

FIGURE 2. The scheme of the adaptive generalized PBC plus damping injection design.

to as the *PBC approach*. The proposed controller regulates the output voltage of second-order DC-DC converters supplying an unknown CPL. Phase portraits, sensitivity analyses, simulations, and experimental results were used to assess the effectiveness of the PBC approach. Furthermore, the proposed control was compared to the feedback linearization control (FLC) and sliding mode control (SMC) approaches. These approaches and their corresponding gain values are described and listed in Section Appendix VI.
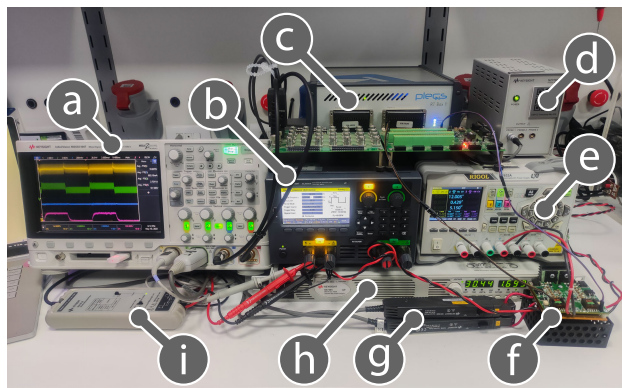
FIGURE 3. Experimental setup: (a) oscilloscope, (b) DC electronic load in constant power mode, (c) RT-Box with analog and digital breakout boards, (d) current probe power supply, (e) MOSFET driver power supply, (f) reconfigurable DC-DC converter, (g) current probes, (h) input voltage power supply, and (i) differential voltage probe.
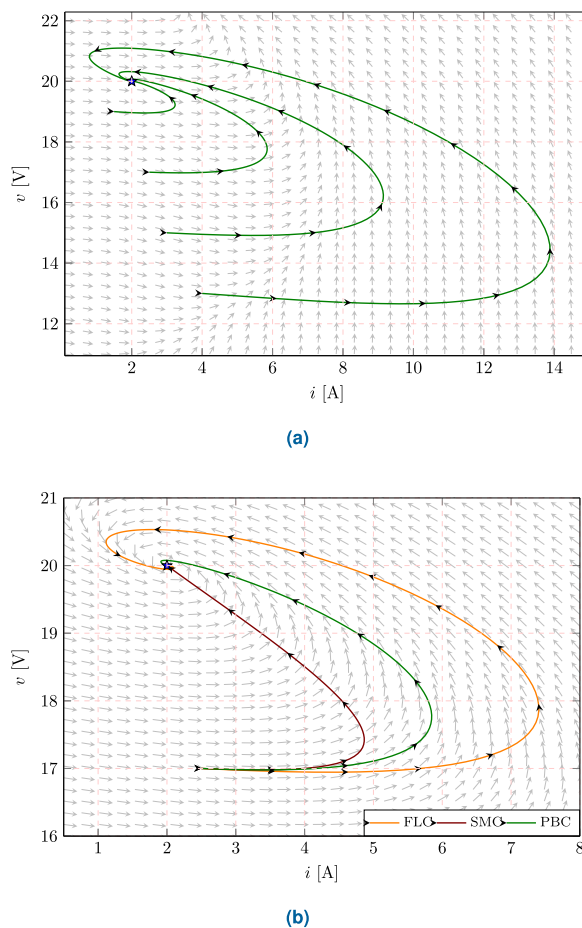
TABLE 3. Components description, reconfigurable power converter.

Component	Description	Type/Value
Q_1 and Q_2	Power MOSFET	IRFB4510PBF
D_1 and D_2	Schottky Power Diode	MBR60H100CTG
L	Inductor	Wurth Elektronik 74435584700, $47~\mu$H
C	Multilayer Ceramic Capacitor	TDK C5750X7S2A106M230KB, $10 \times 10~\mu$F

(a)

(b)

FIGURE 5. Phase portrait for the PBC plus damping injection method implemented in a boost converter: (a) phase portrait with four different initial points, and (b) comparison of the controllers in phase portrait.

(a)

(b)

FIGURE 4. Phase portrait for the PBC plus damping injection method implemented in a buck converter: (a) phase portrait with four different initial points, and (b) comparison of the controllers in phase portrait.

The sensitivity analysis and simulations were conducted using the PLECS software, and the controllers were implemented in the RT-Box of Plexim, as shown in Fig. 3. Table 3 displays a list of components and their corresponding values

for the prototypes. This setup utilizes a reconfigurable converter to obtain various circuits, including buck, boost, buck-boost, and non-inverting buck-boost. The controllers are implemented using hardware in the loop with an RT-BOX 1 from PLECS. Voltage is measured using two probes: one to display the waveform on the oscilloscope and a differential probe to transmit the measurement to the control in the RT-BOX 1. The reason for this is that the analog input of the RT-BOX 1 is passive. Therefore, to obtain an accurate signal in the control, a differential probe powered by batteries is required. The same principle applies to measuring current: one probe is connected to the oscilloscope to display the
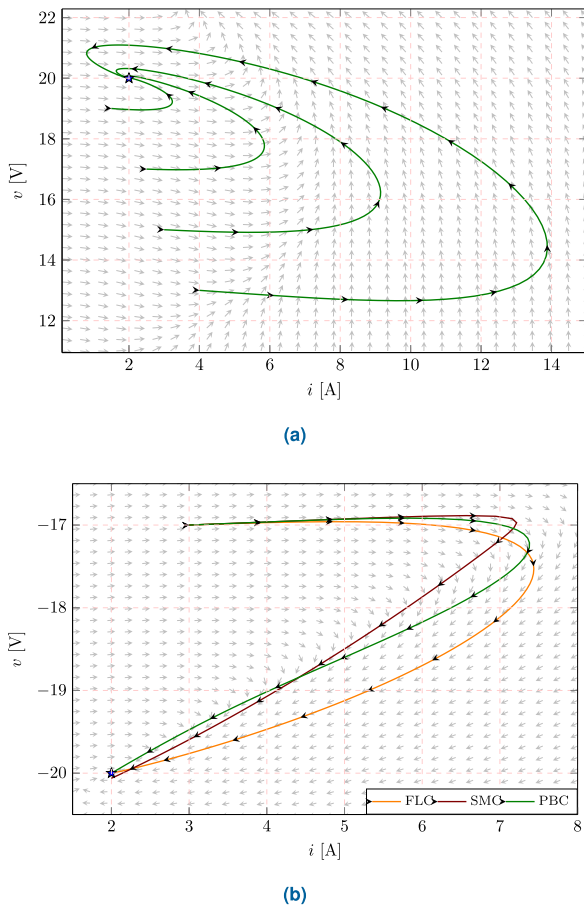
FIGURE 6. Phase portrait for the PBC plus damping injection method implemented in a buck-boost converter: (a) phase portrait with four different initial points, and (b) comparison of the controllers regarding the phase portrait.
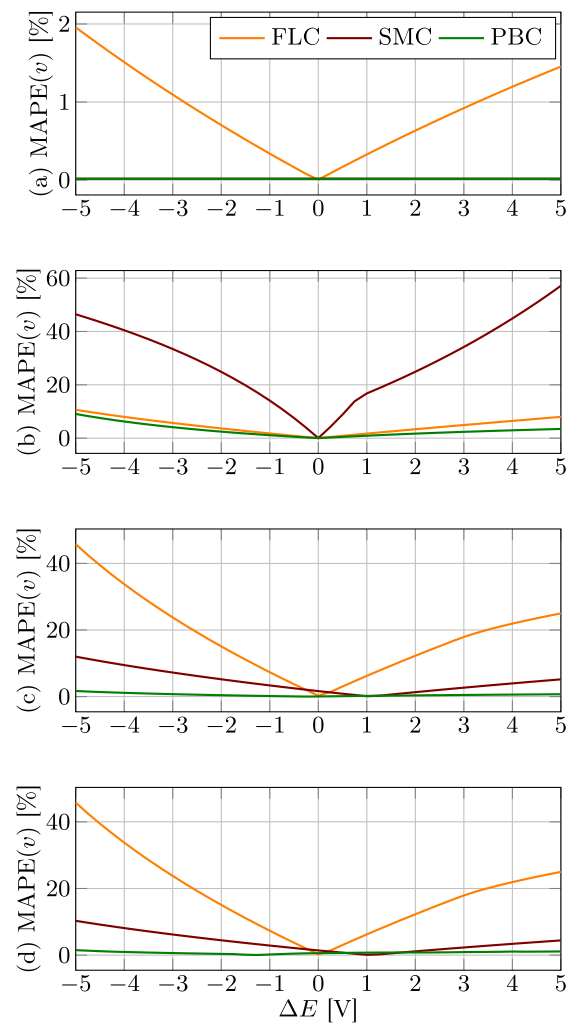

FIGURE 7. Sensitivity analysis for the input voltage E: (a) buck, (b) boost, (c) buck-boost, and (d) non-inverting buck-boost converters

current waveform, while the other one is connected to a power supply to measure the current and transmit the data to the RT-BOX 1.

A. PHASE PORTRAIT ANALYSIS

This section analyzes the behavior of the proposed controller by studying the phase portrait with different initial points. This analysis is only valid for buck, boost, and buck-boost converters, since non-inverting buck-boost converters work similarly to buck-boost ones.

Figs. 4, 5, and 6 illustrate the phase portraits for the buck, boost, and buck-boost converters, respectively, when the proposed controller is implemented. Figs. 4a, 5a, and 6a depict the phase plots of the PBC plus damping injection method and the trajectories for four different initial points. Figs. 4b, 5b, and 6b show the comparison of the trajectories in the phase plot between the proposed controller against FLC and SMC approaches starting from the same point.

The desired equilibrium point (u) for the buck converter regarding its phase portrait (see Fig. 4a) is computed with $E = 30$ V, $P = 20$ W and $v^s = 20$ V. Note that, in Fig. 4a,

different initial points are in ranges 1.5 A $\leq i(0) \leq$ 4 A and 17 V $\leq v(0) \leq$ 19.5 V. This figure shows that, if $v(0) < v^v$, i overshoots and, as $v(0)$ goes far from the desired equilibrium point, the overshoot in the current increases. Fig. 4b shows that the proposed controller and SMC approach have a trajectory similar to that of a linear system, while the FLC approach behaves as a second-order system.

The different initial points for the boost converter are in ranges 1.5 A $\leq i(0) \leq$ 4 A and 17 V $\leq v(0) \leq$ 19.5 V (see Fig. 5a). In this case, the desired equilibrium point ($\star$) is calculated with $E = 10$ V, $P = 20$ W, and $v^\star = 20$ V. In Fig. 5a, it can be observed that, when $v(0) < v^\star$, the current passing through the inductor overshoots, and, similar to that in the buck converter, this overshoot increases as $v(0)$ approaches to E. Additionally, it can also be stated that, as $v(0)$ comes closer to E, the current i exhibits an oscillation around the desired equilibrium point ($\star$), as illustrated in Fig. 5a. Fig. 5b shows that the SMC approach has a more direct trajectory to the desired equilibrium point ($\star$), while the
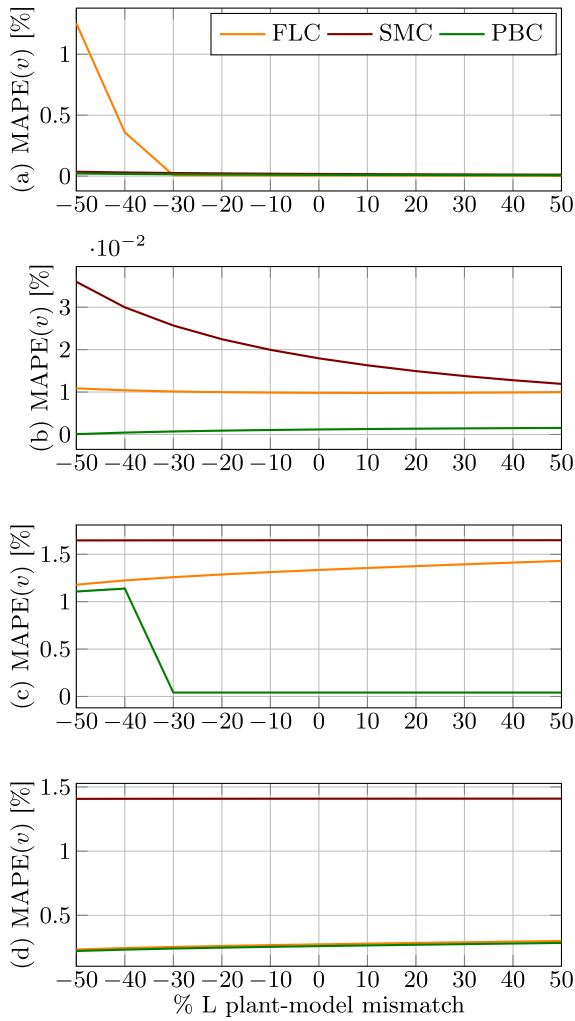
FIGURE 8. Sensitivity analysis for inductance L: (a) buck, (b) boost, (c) buck-boost, and (d) non-inverting buck-boost converters
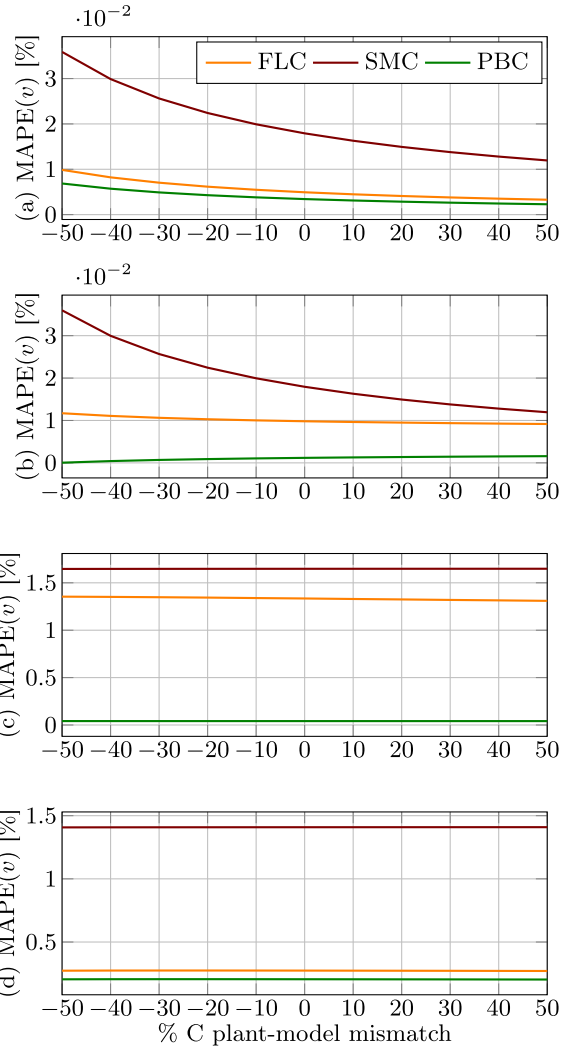
FIGURE 9. Sensitivity analysis for capacitance C: (a) buck, (b) boost, (c) buck-boost, and (d) non-inverting buck-boost converters

proposed controller and the FLC approach behave as second-order systems. However, it is essential to mention that this does not mean that the SMC approach has a faster response than other controllers.

The desired equilibrium point ($\star$) for the buck-boost converter is calculated with $E = 10$ V, $P = 20$ W, and $v^\star = -20$ V. Fig. 6a shows the phase portrait for the buck-boost converter starting at four different points, which are in ranges 1.5 A $\leq i(0) \leq 4$ A and -19 V $\leq v(0) \leq -16$ V. All initial points keep the voltage $v(t)$ constant, while the inductor current increases. This increment becomes greater as $v(0)$ moves further away from $v^\star$. Note that, in Fig. 6b, the SMC approach exhibits a straighter trajectory at the equilibrium point ($\star$). However, it shows little oscillation around this point. The FLC approach is the controller with the smallest voltage rise from the starting point. Nevertheless, in this controller, the inductor current is further away from the equilibrium point. At the same time, the proposed control is the controller with the best convergence at the equilibrium point ($\star$).

Note that, in Figs. 5 and 6, $v(0)$ initially moves away from $v^\star$ and then converges to the desired equilibrium point. This means that the boost and buck-boost converters behave as non-minimum-phase systems.

B. SENSITIVITY ANALYSIS

This section presents a sensitivity analysis aiming to study the impact of variation in the input voltage E and parameters (L, C) on the controllers. The input voltage varies $\pm 5V$ with respect to the real value. It is important to mention that this voltage E is not measured at any moment in this work. At the same time, the parameters (L, C) vary $\pm 50\%$ regarding their rated value. These variations are performed one at a time in order to analyze their effect on the performance of the controllers. The mean absolute percentage error (MAPE) is employed as the performance index. The MAPE(v) is computed as the mean absolute percentage error between the converter output voltage and its desired reference.
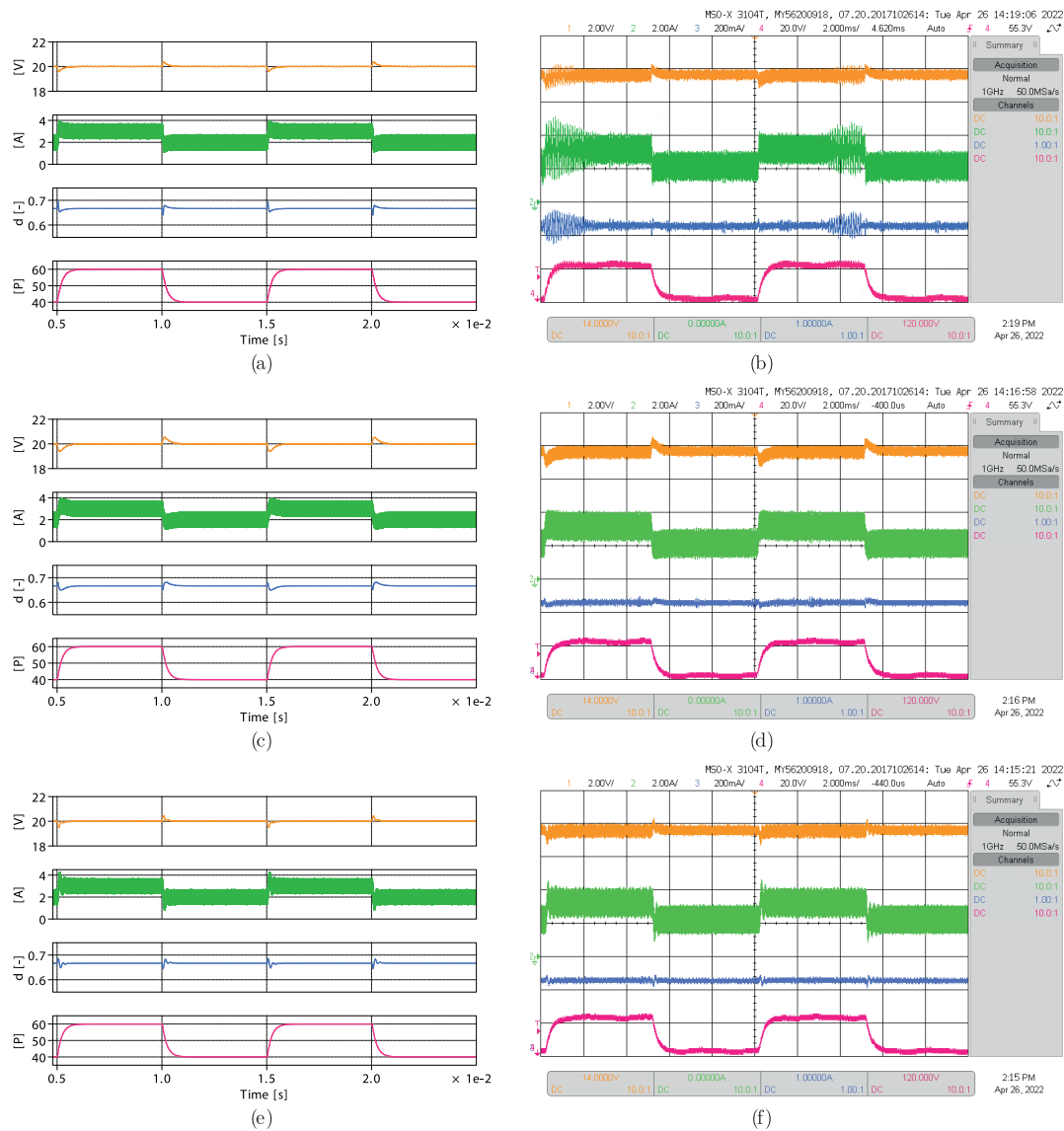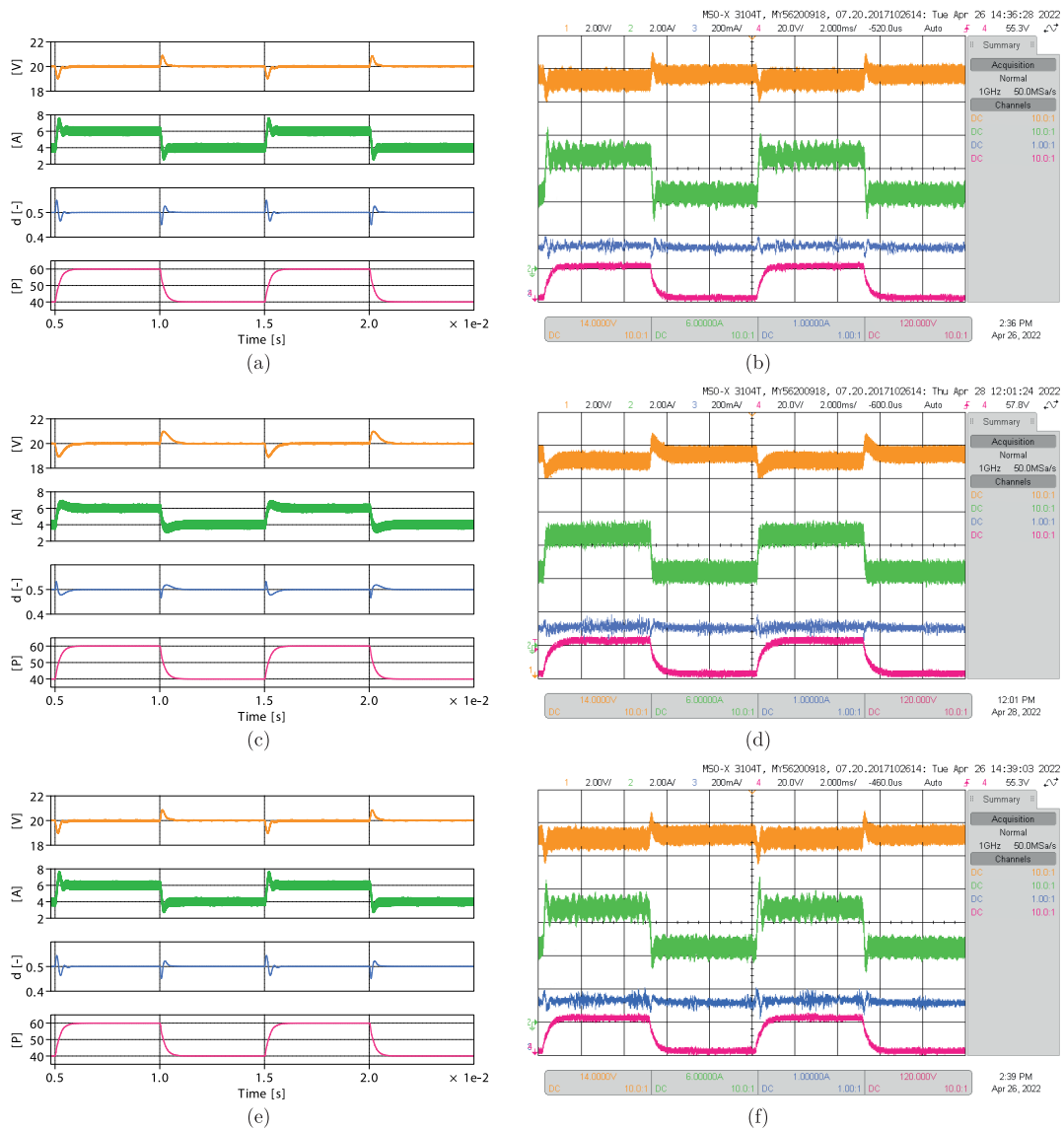
FIGURE 10. Dynamic results for the buck converter when the CPL varies. Simulated responses: (a), (c), and (e); experimental responses: (b), (d), and (f).

Fig. 7 illustrates the sensitivity analysis when the input voltage E varies $\pm 5V$ for all controllers implemented in this paper. Fig. 7a depicts the input voltage variation for the buck converter. In this variation, all controllers respond correctly, but the FLC approach is more affected since it exhibits a linear behavior as the variation grows, reaching 2% of MAPE(v). Fig. 7b shows the MAPE(v) for the boost converter. In this case, the input voltage variation greatly affects the overall controller. However, the proposed controller is the one with the fewest MAPE(v) variations. In contrast, in the worst case, the SMC approach exhibits a greater variation, which exceeds 50% of the MAPE(v). Figs. 7c and 7d display the input voltage variation for the buck-boost and non-inverting buck-boost converters, respectively. For these

converters, the FLC approach shows a great variation as the input voltage variation grows, reaching 40% of the MAPE(v) in the worst case. At the same time, the proposed controller is less affected in all cases, which indicates that it is more robust against these variations.

Fig. 8 shows the sensitivity analysis when the inductance L varies $\pm 50\%$ for all converters implemented in this work. Fig. 8a shows that the PBC and SMC approaches do not undergo any change in their performance when the inductance L varies by $\pm 50\%$ in the buck converter. In contrast, the FLC approach increases its MAPE(v) value when the reduction in inductance L is greater than 30%, thus increasing its steady-state error above 1%. As for the boost converter, the performance of the controllers is not affected by the

FIGURE 11. Dynamic results for the boost converter when the CPL varies. Simulated responses (a), (c), and (e); experimental responses: (b), (d), and (f)

variation in inductance, since the value of the MAPE(v) is less than 0.035%, as shown in Fig. 8b. For the buck-boost and non-inverting buck-boost converters, the performance of the controllers does not change when the variation in inductance is introduced; it remains almost constant in all ranges (see Figs. 8c and 8d). Only the proposed controller is affected when the reduction in inductance L exceeds 30%, increasing its steady-state error by around 1.15%. However, its steady-state error is always less than that of the other controllers.

The results of the sensitivity analysis conducted when the capacitance C varied by $\pm50\%$ is shown in Fig. 9 for all converters implemented in this work. There is no significant change in the performance of the controllers. However, the

PBC approach continues to show that the controller is less affected by variations in the controller parameters or the input voltage than the other controllers. This means that the proposed approach is more robust under changes or uncertainties.

C. RESULTS FOR DC-DC CONVERTERS

This subsection analyzes the performance of all controllers used in this paper. During simulation and experimentation, the controllers operated with a sample time of $10\mu s$. The CPL varied with a frequency of 100 Hz in a square waveform.

Fig. 10 illustrates the results for the buck converter's simulated and experimental responses. This figure shows the results for the FLC (Figs. 10a and 10b), SMC
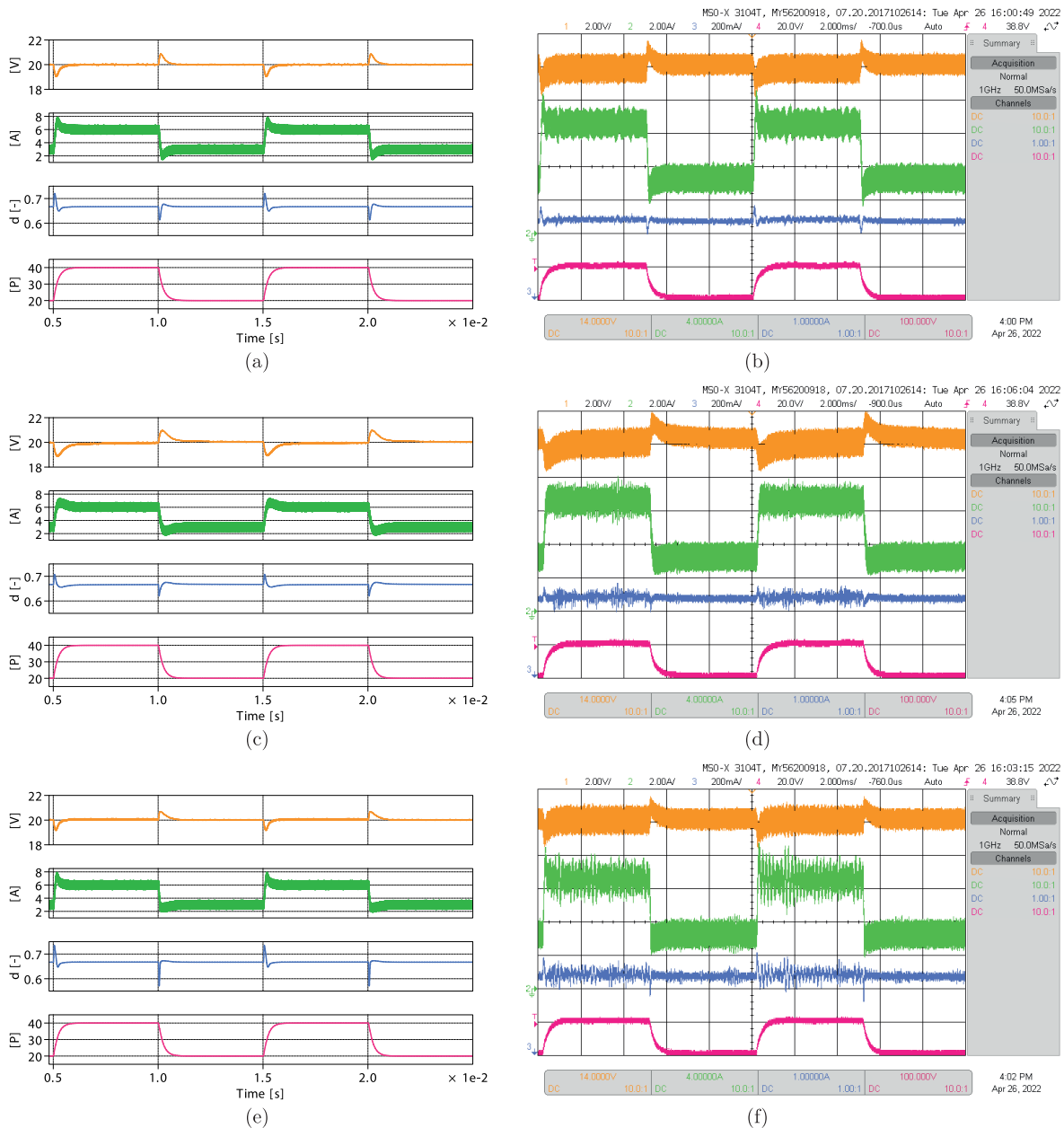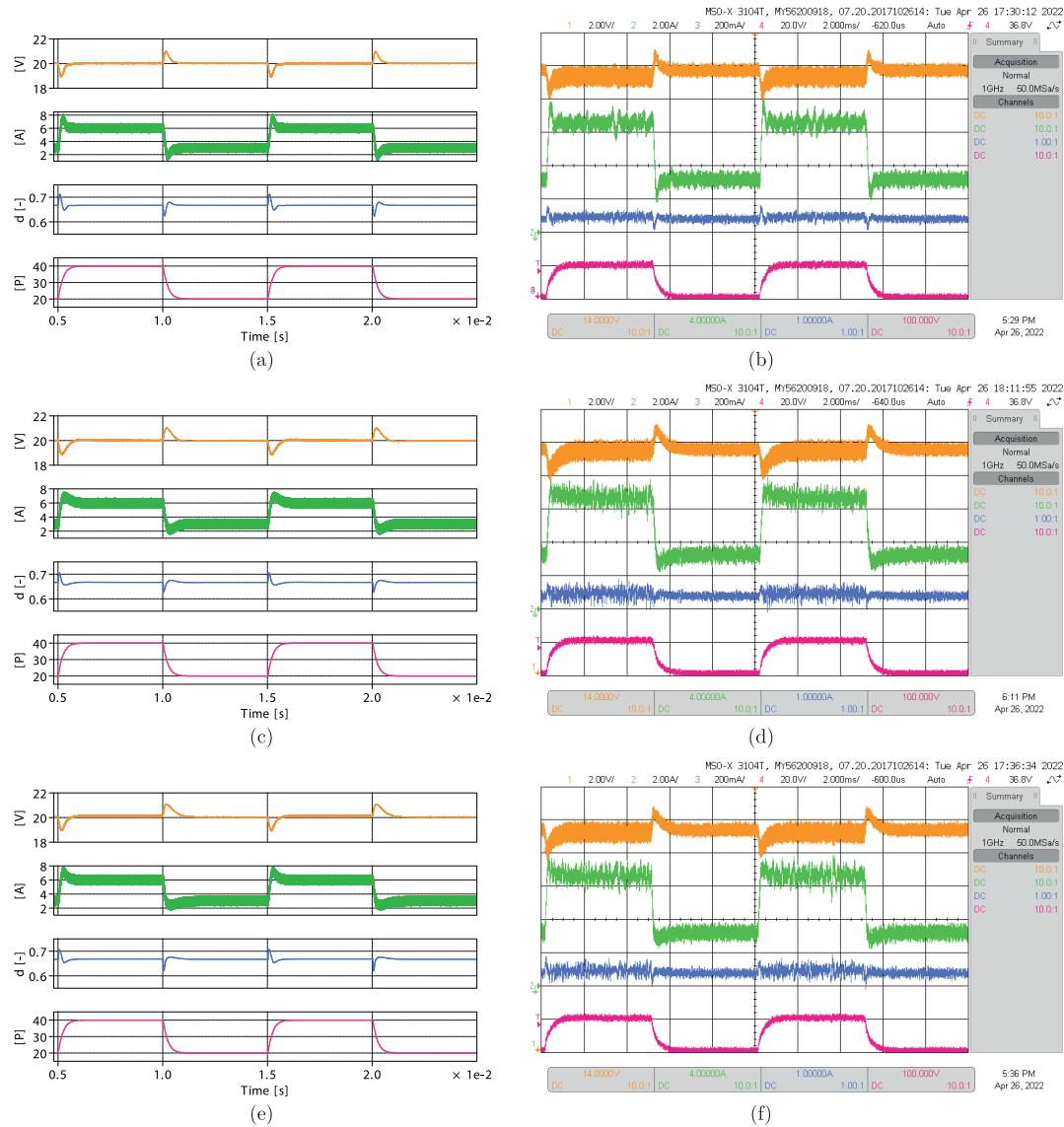
FIGURE 12. Dynamic results for the buck-boost converter when the CPL varies. Simulated responses (a), (c), and (e); experimental responses: (b), (d), and (f).

(Figs. 10c and 10d), and PBC approaches (Figs. 10e and 10f). In this case, the input voltage for the buck converter is $E = 30$ V, and the CPL changes from 40 to 60 W and *vice versa*. The SMC approach is the worst controller with regard to the settling time ($T_s = 831.88 \mu$s). Furthermore, the SMC approach is the controller with the largest voltage overshoot (around 3.5%). While it was a little slower than the FLC approach, it had the lowest voltage overshoot (around 1.8%). Fig. 10b shows that the FLC approach exhibits a high ripple in the inductor current, unlike the other approaches. In general

terms, all of the above indicates that the proposed controller has a better dynamical response than the others.

Fig. 11 shows the simulation and experimental results for the boost converter feeding a CPL. This figure presents the dynamic results for the FLC (Figs. 11a and 11b), SMC (Figs. 11c and 11d), and PBC approaches (Figs. 11e and 11f). For the boost converter, the input voltage is $E = 10$ V, and the CPL varies between 40 and 60 W and *vice versa*. The SMC approach exhibits the worst performance with respect to the settling time ($T_s = 1189.38 \mu$s). While the FLC approach

FIGURE 13. Dynamic results for the non-inverting buck-boost converter when the CPL varies. Simulated responses (a), (c), and (e); experimental responses: (b), (d), and (f).

shows the worst voltage overshoot (around 6.1 %), it has the best settling time ($T_s = 591.25\mu$s), but it has a greater voltage overshoot than the PBC approach. In addition, its dynamic response contains more oscillations than the other approaches. The proposed adaptive controller continues to perform better than the FLC and SMC approaches.

Fig. 12 presents the simulation and experimental results for the buck-boost converter when it is supplying an unknown CPL. The figure depicts the dynamic results for the FLC (Figs. 12a and 12b), SMC (Figs. 12c and 12d), and PBC (Figs. 12e and 12f) approaches. For the buck-boost converter, the input voltage is $E = 10$ V, the CPL varies between 20 and 40 W, and the output voltage reference is $v^\star = -20$ V. The FLC and PBC approaches show the same settling time

($T_s = 880\mu$s), whereas the SMC has a longer settling time ($T_s = 1340.63\mu$s), about 47.7% that of other approaches. The PBC approach exhibits a lower voltage overshoot (3.5%) than the FLC (4.8%), and SMC (4.6%) approaches. The indices (settling time and voltage overshoot) demonstrate that the adaptive proposed controller performs better than the others.

Fig. 13 illustrates the simulation and experimental results for the non-inverting buck-boost converter when an unknown CPL is fed. The figure shows the results for the FLC (Figs. 13a and 13b), SMC (Figs. 13c and 13d), and PBC (Figs. 13e and 13f) approaches. For the non-inverting buck-boost converter, the input voltage is $E = 10$ V, the CPL varies between 20 and 40 W, and the output voltage reference is $v^\star = 20$ V. The SMC approach has the worst performance

TABLE 4. Summary of indices for each controller.

Controller	Settling time (μs)	Reduction (%)	Voltage overshoot (%)	Reduction (%)
		Buck converter		
FLC	522.5	62.8	2.04	58.3
SMC	831.8	–	3.5	–
PBC	564.38	67.8	1.8	51.4
		Boost converter		
FLC	591.2	20.28	6.1	–
SMC	1189.3	–	4.1	32.7
PBC	545.6	54.1	3.1	49.2
		Buck-boost converter		
FLC	880	34.4	4.8	–
SMC	1340.6	–	4.6	4.2
PBC	880	34.4	3.5	27.1
		Non-inverting buck-boost converter		
FLC	749.3	43.5	4.8	23.8
SMC	1326.2	–	6.3	–
PBC	750	43.4	3.5	44.4

All reduction from the worst performance

TABLE 5. Parameter values for the control actions.

FLC approach	
Converter	Parameters
Buck	$k_1 = 5, k_2 = 2C$
Boost	$k_1 = 1/L, k_2 = 22.7, k_z = 20$
Buck-boost	$k_1 = 1.5/L, k_2 = 3, k_z = 0.01$
Non-inverting buck-boost	$k_1 = 1/L, k_2 = 3, k_z = 100$
SMC approach	
Converter	Parameters
Buck	$Q = 0.1, \lambda = 1, \mu = 60$
Boost	$Q = 3, \lambda = 1000, \mu = 25$
Buck-boost	$Q = 150, \lambda = 8000, k_1 = 4.9,$ $k_2 = -30, k_z = -1000$
Boost	$Q = 3, \lambda = 1000, \mu = 25$
Non-inverting buck-boost	$Q = 15, \lambda = 8000, k_1 = 3.43,$ $k_2 = -17.5, k_z = -2000$
PBC approach	
Converter	Parameters
Buck	$R_1 = 1, R_2 = 20, K = 0.003$
Boost	$R_1 = 0.025, R_2 = 7, K = 0.006$
Buck-boost	$R_1 = 0.08, R_2 = 12.6, K = 0.01$
Non-inverting buck-boost	$R_1 = 0.1, R_2 = 2, K = 0.005$

regarding the settling time ($T_s = 1326.28 \mu$s) and voltage overshoot (6.3 %). Meanwhile, the FLC approach has the best settling time ($T_s = 749.38 \mu$s), but it has a voltage overshoot greater than the PBC approach.

Finally, Table 4 presents a summary of the settling time and overshoot in the output voltage of each controller. This table shows that overall, the adaptive proposed controller had a better performance than the other controllers, which makes it suitable for implementation in any second-order converter and has superior performance. Additionally, the proposed controller can guarantee the converter's stability.

VI. CONCLUSION

This paper developed a generalized PBC approach to regulate the output voltage of second-order DC-DC converters supplying an unknown CPL. The generalized PBC approach added damping injection to stabilize DC-DC converters while imposing the desired damping. Furthermore, the I&I method was integrated into the proposed controller in order to transform it into a generalized adaptive control approach that ensures local asymptotic stability for each converter. The adaptive control approach does not depend on the converter parameters, which makes it robust against parameter uncertainties. The robustness and effectiveness of the proposed PBC approach were evaluated via phase portrait and sensitivity analyses, as well as from simulation and experimental results. The set of all these analyses, along with a comparison against the FLC and SMC approaches, supports the superior performance of the proposed controller.

APPENDIX A DESIGN OF OTHER NONLINEAR CONTROLS

This Appendix shows the design of control actions based on the FLC and SMC approaches for each DC-DC converter considered in this paper. The following control actions are presented used for the sake of comparison with the proposed controller:

i *Buck converter*

$$FLC \begin{cases} u = \dfrac{w - L\hat{P}\frac{i-\hat{P}/v}{Cv^2}}{E} + \dfrac{v}{E}, \\ w = -k_1(v - v^\star) - \dfrac{k_2}{C}\left(i - \hat{P}/v^\star\right). \end{cases} \quad (39)$$

$$SMC \begin{cases} u = \dfrac{v}{E} - \dfrac{L}{Ev}\left(\dfrac{(i+\mu)(i - \hat{P}/v)}{C} + \dfrac{\lambda s + Q\,|s|}{L}\right), \\ s = iv - \hat{P} + \mu(v - v^\star). \end{cases} \quad (40)$$

Boost converter

$$FLC \begin{cases} u = 1 + \dfrac{Lw - E}{v}, \\ w = -k_1\left(i - \left(\dfrac{\hat{P}}{E} - k_2(v - v^\star) - k_i z\right)\right), \\ \dot{z} = v - v^\star. \end{cases} \quad (41)$$

$$SMC \begin{cases} u = 1 - \dfrac{\hat{P}(i+\mu)/(Cv) - \lambda s - Q\,|s|}{(i+\mu)i/C - v^2/L}, \\ s = iv - \dfrac{v^\star \hat{P}}{E} + \mu(v - v^\star). \end{cases} \quad (42)$$

Buck-boost converter

$$FLC \begin{cases} u = \dfrac{Lw - v}{E - v}, \\ w = k_1\left(\hat{P}\left(\dfrac{1}{E} - \dfrac{1}{v}\right) + k_2(v - v^\star) + k_i z - i\right), \\ \dot{z} = v - v^\star. \end{cases} \quad (43)$$

$$SMC \begin{cases} u = \dfrac{k_2(i + \hat{P}/(Cv)) - k_1 v/L - k_z \dot{z} - \lambda s - Q\,|s|}{k_1(E - v)/L + k_2 i/C}, \\ s = k_1\left(i - \hat{P}\left(\dfrac{1}{E} - \dfrac{1}{v^\star}\right)\right) + k_2(v - v^\star) + k_i z, \\ \dot{z} = v - v^\star. \end{cases} \quad (44)$$

By changing the sign of the output voltage and its reference to the control actions in (43) and (44), they can be used for the non-inverting buck-boost converter. Table 5 lists the parameter values for the control actions based on the FLC and SMC approaches.

REFERENCES

[1] A. Valencia, R. A. Hincapie, and R. A. Gallego, "Optimal location, selection, and operation of battery energy storage systems and renewable distributed generation in medium–low voltage distribution networks," *J. Energy Storage*, vol. 34, Feb. 2021, Art. no. 102158.

[2] J. A. P. Lopes, A. Madureira, N. Gil, and F. Resende, "Operation of multi-microgrids," in *Microgrids*. Hoboken, NJ, USA: Wiley, Dec. 2013, pp. 165–205.

[3] K. López-Rodríguez, W. Gil-González, and A. Escobar-Mejía, "Design and implementation of a PI-PBC to manage bidirectional power flow in the DAB of an SST," *Results Eng.*, vol. 14, Jun. 2022, Art. no. 100437.

[4] V. Anand and V. Singh, "Compact symmetrical and asymmetrical multilevel inverter with reduced switches," *Int. Trans. Electr. Energy Syst.*, vol. 30, no. 8, p. e12458, Aug. 2020.

[5] O. D. Montoya, W. Gil-González, and A. Garces, "Numerical methods for power flow analysis in DC networks: State of the art, methods and challenges," *Int. J. Electr. Power Energy Syst.*, vol. 123, Dec. 2020, Art. no. 106299.

[6] W. Gil-González, O. D. Montoya, E. Holguín, A. Garces, and L. F. Grisales-Noreña, "Economic dispatch of energy storage systems in DC microgrids employing a semidefinite programming model," *J. Energy Storage*, vol. 21, pp. 1–8, Feb. 2019.

[7] J.-O. Lee, Y.-S. Kim, and J.-H. Jeon, "Generic power flow algorithm for bipolar DC microgrids based on Newton–Raphson method," *Int. J. Electr. Power Energy Syst.*, vol. 142, Nov. 2022, Art. no. 108357.

[8] W. He, M. M. Namazi, H. R. Koofigar, M. A. Amirian, and F. Blaabjerg, "Stabilization of DC–DC buck converter with unknown constant power load via passivity-based control plus proportion-integration," *IET Power Electron.*, vol. 14, no. 16, pp. 2597–2609, Dec. 2021.

[9] G. L. Magaldi, F. M. Serra, C. H. de Angelo, O. D. Montoya, and D. A. Giral-Ramírez, "Voltage regulation of an isolated DC microgrid with a constant power load: A passivity-based control design," *Electronics*, vol. 10, no. 17, p. 2085, Aug. 2021.

[10] V. Anand, V. Singh, and J. S. M. Ali, "Dual boost five-level switched-capacitor inverter with common ground," *IEEE Trans. Circuits Syst. II, Exp. Briefs*, vol. 70, no. 2, pp. 556–560, Feb. 2023.

[11] Z. Xia, M. Su, Z. Liu, R. Liu, and Y. Liu, "Existence conditions and stability for the power-flow of DC micro-grids with CPLs," *IEEE Trans. Smart Grid*, vol. 13, no. 6, pp. 4284–4299, Nov. 2022.

[12] O. D. Montoya, W. Gil-González, A. Garces, F. Serra, and J. C. Hernández, "Stabilization of MT-HVDC grids via passivity-based control and convex optimization," *Electr. Power Syst. Res.*, vol. 196, Jul. 2021, Art. no. 107273.

[13] M. Jeeninga, C. De Persis, and A. van der Schaft, "DC power grids with constant-power loads—Part II: Nonnegative power demands, conditions for feasibility, and high-voltage solutions," *IEEE Trans. Autom. Control*, vol. 68, no. 1, pp. 18–30, Jan. 2023.

[14] V. Anand and V. Singh, "A 13-level switched-capacitor multilevel inverter with single DC source," *IEEE J. Emerg. Sel. Topics Power Electron.*, vol. 10, no. 2, pp. 1575–1586, Apr. 2022.

[15] D. K. Fulwani and S. Singh, "Introduction," in *Mitigation of Negative Impedance Instabilities in DC Distribution Systems*. Singapore: Springer, Oct. 2016, pp. 1–33.

[16] W. Gil-González, O. D. Montoya, C. Restrepo, and J. C. Hernández, "Sensorless adaptive voltage control for classical DC–DC converters feeding unknown loads: A generalized PI passivity-based approach," *Sensors*, vol. 21, no. 19, p. 6367, Sep. 2021.

[17] M. Jeeninga, "Braess' paradox for power flow feasibility and parametric uncertainties in DC power grids with constant-power loads," *Syst. Control Lett.*, vol. 161, Mar. 2022, Art. no. 105146.

[18] S. Bacha, I. Munteanu, and A. I. Bratcu, "Linear control approaches for DC–DC power converters," in *Power Electronic Converters Modeling and Control*. London, U.K.: Springer, Sep. 2013, pp. 187–236.

[19] S. Singh, D. Fulwani, and V. Kumar, "Robust sliding-mode control of DC/DC boost converter feeding a constant power load," *IET Power Electron.*, vol. 8, no. 7, pp. 1230–1237, Jul. 2015.

[20] A. Subramanian and U. Govindarajan, "Analysis and mitigation of conducted EMI in current mode controlled DC–DC converters," *IET Power Electron.*, vol. 12, no. 4, pp. 667–675, Feb. 2019.

[21] S. Singh and D. Fulwani, "Voltage regulation and stabilization of DC/DC buck converter under constant power loading," in *Proc. IEEE Int. Conf. Power Electron., Drives Energy Syst. (PEDES)*, Dec. 2014, pp. 1–6.

[22] M. K. Al-Nussairi, R. Bayindir, and E. Hossain, "Fuzzy logic controller for DC–DC buck converter with constant power load," in *Proc. IEEE 6th Int. Conf. Renew. Energy Res. Appl. (ICRERA)*, Nov. 2017, pp. 1175–1179.

[23] Q. Xu, Y. Yan, C. Zhang, T. Dragicevic, and F. Blaabjerg, "An offset-free composite model predictive control strategy for DC/DC buck converter feeding constant power loads," *IEEE Trans. Power Electron.*, vol. 35, no. 5, pp. 5331–5342, May 2020.

[24] M. Boukerdja, A. Chouder, L. Hassaine, B. O. Bouamama, W. Issa, and K. Louassaa, "H_∞-based control of a DC/DC buck converter feeding a constant power load in uncertain DC microgrid system," *ISA Trans.*, vol. 105, pp. 278–295, Oct. 2020.

[25] B. Singh and M. K. Singh, "Adaptive energy shaping control of buck converter feeding CPL in DC micro-grid system," in *Proc. IEEE 2nd Int. Conf. Smart Technol. Power, Energy Control (STPEC)*, Dec. 2021, pp. 1–5.

[26] W. He, M. M. Namazi, H. R. Koofigar, M. A. Amirian, and J. M. Guerrero, "Voltage regulation of buck converter with constant power load: An adaptive power shaping control," *Control Eng. Pract.*, vol. 115, Oct. 2021, Art. no. 104891.

[27] M. S. Ali, M. Soliman, A. M. Hussein, and S. A. F. Hawash, "Robust controller of buck converter feeding constant power load," *J. Control, Autom. Electr. Syst.*, vol. 32, no. 1, pp. 153–164, Feb. 2021.

[28] C. Cui, N. Yan, B. Huangfu, T. Yang, and C. Zhang, "Voltage regulation of DC–DC buck converters feeding CPLs via deep reinforcement learning," *IEEE Trans. Circuits Syst. II, Exp. Briefs*, vol. 69, no. 3, pp. 1777–1781, Mar. 2022.

[29] O. Kaplan and F. Bodur, "Second-order sliding mode controller design of buck converter with constant power load," *Int. J. Control*, vol. 96, no. 5, pp. 1–17, 2022.

[30] A. M. Abdurraqeeb, A. A. Al-Shamma'a, A. Alkuhayli, A. M. Noman, and K. E. Addoweesh, "RST digital robust control for DC/DC buck converter feeding constant power load," *Mathematics*, vol. 10, no. 10, p. 1782, May 2022.

[31] S. A. G. K. Abadi, T. Khalili, S. I. Habibi, A. Bidram, and J. M. Guerrero, "Adaptive control and management of multiple nano-grids in an islanded DC microgrid system," *IET Gener., Transmiss. Distrib.*, vol. 17, no. 8, pp. 1799–1815, Apr. 2023.

[32] S. A. Hamidi and A. Nasiri, "Stability analysis of a DC–DC converter for battery energy storage system feeding CPL," in *Proc. IEEE Int. Telecommun. Energy Conf. (INTELEC)*, Oct. 2015, pp. 1–5.

[33] J. Wu and Y. Lu, "Adaptive backstepping sliding mode control for boost converter with constant power load," *IEEE Access*, vol. 7, pp. 50797–50807, 2019.

[34] W. He, S. Li, J. Yang, and Z. Wang, "Incremental passivity based control for DC–DC boost converter with circuit parameter perturbations using nonlinear disturbance observer," in *Proc. 42nd Annu. Conf. IEEE Ind. Electron. Soc. (IECON)*, Oct. 2016, pp. 1353–1358.

[35] W. He, S. Li, J. Yang, and Z. Wang, "Incremental passivity based control for DC–DC boost converters under time-varying disturbances via a generalized proportional integral observer," *J. Power Electron.*, vol. 18, no. 1, pp. 147–159, 2018.

[36] B. A. Martinez-Treviño, A. El Aroudi, E. Vidal-Idiarte, A. Cid-Pastor, and L. Martinez-Salamero, "Sliding-mode control of a boost converter under constant power loading conditions," *IET Power Electron.*, vol. 12, no. 3, pp. 521–529, Mar. 2019.

[37] H. Farsizadeh, M. Gheisarnejad, M. Mosayebi, M. Rafiei, and M. H. Khooban, "An intelligent and fast controller for DC/DC converter feeding CPL in a DC microgrid," *IEEE Trans. Circuits Syst. II, Exp. Briefs*, vol. 67, no. 6, pp. 1104–1108, Jun. 2020.

[38] W. He and Y. Shang, "Finite-time parameter observer-based sliding mode control for a DC/DC boost converter with constant power loads," *Electronics*, vol. 11, no. 5, p. 819, Mar. 2022.

[39] X. Zhang, W. He, and Y. Zhang, "An adaptive output feedback controller for boost converter," *Electronics*, vol. 11, no. 6, p. 905, Mar. 2022.

[40] X. Zhang, M. Martinez-Lopez, W. He, Y. Shang, C. Jiang, and J. Moreno-Valenzuela, "Sensorless control for DC–DC boost converter via generalized parameter estimation-based observer," *Appl. Sci.*, vol. 11, no. 16, p. 7761, Aug. 2021.

[41] W. Gil-González, O. D. Montoya, S. Riffo, C. Restrepo, and J. Muñoz, "A global tracking sensorless adaptive PI-PBC design for output voltage regulation in a boost converter feeding a DC microgrid," *Energies*, vol. 16, no. 3, p. 1106, Jan. 2023.

[42] S. Riffo, W. Gil-González, O. D. Montoya, C. Restrepo, and J. Muñoz, "Adaptive sensorless PI+Passivity-based control of a boost converter supplying an unknown CPL," *Mathematics*, vol. 10, no. 22, p. 4321, Nov. 2022.

[43] W. He, C. A. Soriano-Rangel, R. Ortega, A. Astolfi, F. Mancilla-David, and S. Li, "Energy shaping control for buck–boost converters with unknown constant power load," *Control Eng. Pract.*, vol. 74, pp. 33–43, May 2018.

[44] W. He, R. Ortega, J. E. Machado, and S. Li, "An adaptive passivity-based controller of a buck–boost converter with a constant power load," *Asian J. Control*, vol. 21, no. 1, pp. 581–595, Jan. 2019.

[45] M. Hajihosseini, M. Andalibi, M. Gheisarnejad, H. Farsizadeh, and M. Khooban, "DC/DC power converter control-based deep machine learning techniques: Real-time implementation," *IEEE Trans. Power Electron.*, vol. 35, no. 10, pp. 9971–9977, Oct. 2020.

[46] M. Gheisarnejad, H. Farsizadeh, M. Tavana, and M. H. Khooban, "A novel deep learning controller for DC–DC buck–boost converters in wireless power transfer feeding CPLs," *IEEE Trans. Ind. Electron.*, vol. 68, no. 7, pp. 6379–6384, Jul. 2021.

[47] C. A. Soriano-Rangel, W. He, F. Mancilla-David, and R. Ortega, "Voltage regulation in buck–boost converters feeding an unknown constant power load: An adaptive passivity-based control," *IEEE Trans. Control Syst. Technol.*, vol. 29, no. 1, pp. 395–402, Jan. 2021.

[48] M. Andalibi, M. Hajihosseini, M. Gheisarnejad, M.-H. Khooban, and J. Boudjadar, "A novel method for stabilizing buck–boost converters with CPL using model prediction control," in *Proc. 22nd IEEE Int. Conf. Ind. Technol. (ICIT)*, vol. 1, Mar. 2021, pp. 541–545.

[49] M. Martinez-Lopez, J. Moreno-Valenzuela, and W. He, "A robust nonlinear PI-type controller for the DC–DC buck–boost power converter," *ISA Trans.*, vol. 129, pp. 687–700, Oct. 2022.

[50] P. C. Papageorgiou and A. T. Alexandridis, "Voltage stabilization of DC/DC converter-driven constant power loads via feeding-back the output measured current," *IFAC-PapersOnLine*, vol. 53, no. 2, pp. 13442–13447, 2020.

[51] B. A. Martínez-Treviño, A. E. Aroudi, and L. Martínez-Salamero, "Sliding-mode approach for start-up control and voltage regulation of a boost converter driving a constant power load," in *Proc. IEEE Int. Symp. Circuits Syst. (ISCAS)*, May 2017, pp. 1–4.

[52] S. Singh, N. Rathore, and D. Fulwani, "Mitigation of negative impedance instabilities in a DC/DC buck–boost converter with composite load," *J. Power Electron.*, vol. 16, no. 3, pp. 1046–1055, May 2016.

[53] A. Khaligh, S. Williamson, and A. Emadi, "Control and stabilization of DC/DC buck–boost converters loaded by constant power loads in vehicular systems using a novel digital scheme," in *Proc. 12th Int. Power Electron. Motion Control Conf.*, Aug. 2006, pp. 1769–1775.

[54] S. Fan, F. Wu, and H. Liu, "Unified closed-loop control and parameters design of buck–boost current-fed isolated DC–DC converter with constant power load," *IEEE J. Emerg. Sel. Topics Power Electron.*, vol. 10, no. 4, pp. 4207–4217, Aug. 2022.

[55] O. Boutebba, S. Semcheddine, F. Krim, F. Corti, A. Reatti, and F. Grasso, "A nonlinear back-stepping controller of DC–DC non inverting buck–boost converter for maximizing photovoltaic power extraction," in *Proc. IEEE Int. Conf. Environ. Electr. Eng., IEEE Ind. Commercial Power Syst. Eur. (EEEIC/I&CPS Europe)*, Jun. 2020, pp. 1–6.

[56] B. Tomescu and H. F. V. Landingham, "On the use of fuzzy logic to control paralleled DC–DC converters," in *Soft Computing in Industrial Electronics*. Heidelberg, Germany: Springer, 2002, pp. 137–195.

[57] J. S. Gómez-Chitiva, A. F. Escalante-Sarrias, and O. D. Montoya, "Voltage regulation in second-order DC–DC converters via the inverse optimal control design with proportional-integral action," *TecnoLógicas*, vol. 25, no. 55, p. e2369, Nov. 2022.

[58] S. Bingqing, Z. Zhengming, W. Shusheng, N. Jintong, and L. Yunzhi, "Load-current sensorless sliding-predictive control strategies for boost converters," *J. Tsinghua Univ., Sci. Technol.*, vol. 59, no. 10, p. 807, 2019.

[59] M. Villegas-Ruvalcaba, K. Gurubel-Tun, and A. Coronado-Mendoza, "Robust inverse optimal control for a boost converter," *Energies*, vol. 14, no. 9, p. 2507, Apr. 2021.

[60] Z. Zhang, G. Song, J. Zhou, X. Zhang, B. Yang, C. Liu, and J. M. Guerrero, "An adaptive backstepping control to ensure the stability and robustness for boost power converter in DC microgrids," *Energy Rep.*, vol. 8, pp. 1110–1124, Jul. 2022.

[61] R. Ortega and E. García-Canseco, "Interconnection and damping assignment passivity-based control: A survey," *Eur. J. Control*, vol. 10, no. 5, pp. 432–450, Jan. 2004.

[62] R. Ortega, A. van der Schaft, F. Castanos, and A. Astolfi, "Control by interconnection and standard passivity-based control of port-Hamiltonian systems," *IEEE Trans. Autom. Control*, vol. 53, no. 11, pp. 2527–2542, Dec. 2008.

[63] F. M. Serra, C. H. De Angelo, and D. G. Forchetti, "IDA-PBC control of a three-phase front-end converter," in *Proc. 38th Annu. Conf. IEEE Ind. Electron. Soc. (IECON)*, Oct. 2012, pp. 5203–5208.

[64] R. Ortega, A. Donaire, and J. G. Romero, "Passivity-based control of mechanical systems," in *Feedback Stabilization of Controlled Dynamical Systems*. Cham, Switzerland: Springer, 2017, pp. 167–199.

[65] T. S. Nguyen, N. H. Hoang, C. K. Tan, and M. A. Bin Hussain, "Proportional-integral passivity-based control design of perturbed nonstandard Hamiltonian systems," *IFAC-PapersOnLine*, vol. 54, no. 19, pp. 19–24, 2021.

[66] L. Perko, *Differential Equations and Dynamical Systems*, vol. 7. New York, NY, USA: Springer, 2001.

[67] A. Astolfi, D. Karagiannis, and R. Ortega, *Nonlinear and Adaptive Control With Applications*, vol. 187. London, U.K.: Springer-Verlag, 2008.

WALTER GIL-GONZÁLEZ (Senior Member, IEEE) was born in Pereira, Colombia, in 1986. He received the B.Sc., M.Sc., and Ph.D. degrees in electrical engineering from Universidad Tecnológica de Pereira, Colombia, in 2011, 2013, and 2019, respectively. He was an Adjunct Professor with Institución Universitaria Pascual Bravo. He is currently an Assistant Professor with the Department of Electric Power Engineering, Universidad Tecnológica de Pereira. His research interests include power systems control and stability and optimization and operation of the power systems.

SEBASTIÁN RIFFO was born in Linares, Chile. He received the bachelor's degree in civil engineering and mechatronics from Universidad de Talca, Curicó, Chile, in 2021, where he is currently pursuing the master's degree in engineering sciences with an emphasis on energy conversion with the Department of Engineering. He is also a part of the Laboratory of Applications in Smart Grids (LARI), research group, led by Prof. Carlos Restrepo. His main research interests include digital control and DC microgrids.

OSCAR DANILO MONTOYA (Senior Member, IEEE) was born in Obando, Valle, Colombia, in 1989. He received the B.E.E., M.Sc., and Ph.D. degrees in electrical engineering from Universidad Tecnológica de Pereira, Colombia, in 2012, 2014, and 2019, respectively. He is currently an Assistant Professor with the Electrical Engineering Program, Universidad Distrital Francisco José de Caldas, Colombia. His research interests include mathematical optimization, planning and control of power systems, renewable energies, energy storage, protective devices, passivity-based control, and dynamical analysis.

Delft, The Netherlands. From 2014 to 2016, he was a Professor with the Department of Electrical Engineering, Universidad Técnica Federico Santa María, Santiago de Chile, Chile. He is currently a Professor with the Department of Electrical Engineering, Universidad de Talca, Curicó, Chile. He is also the Director of the Laboratory of Applications in Smart Grids (LARI), research group. His research interests include modeling and emulator design for fuel cells, design and digital control of switched converters, and energy management of hybrid electric vehicles.

CARLOS RESTREPO received the bachelor's (Hons.) and master's degrees in electrical engineering from Universidad Tecnológica de Pereira, Pereira, Colombia, in 2006 and 2007, respectively, and the master's and Ph.D. (Hons.) degrees in electronic engineering from Universitat Rovira i Virgili de Tarragona, Tarragona, Spain, in 2008 and 2012, respectively. He was a Visiting Scholar with the Faculty of Electrical Engineering and Computer Science, University of Maribor, Maribor, Slovenia, in 2011. In 2013 and 2014, he was a Postdoctoral Researcher with the Electrical Power Processing Group, Delft University of Technology,

JESÚS C. HERNÁNDEZ (Member, IEEE) was born in Jaén, Spain. He received the M.Sc. and Ph.D. degrees from the University of Jaén, in 1994 and 2003, respectively. Since 2023, he has been a Full Professor with the Department of Electrical Engineering, University of Jaén. His current research interests include smart grids, smart meters, renewable energy, and power electronics.

● ● ●